



Insights into the chemical and physical drivers of surface ozone in the Trans-Himalaya

Imran A. Girach^{1,*}, Mehul R. Pandya¹, Tabish Ansari², Sonam Angmo³, Subrat Sharma^{4,5}, Bipasha Paul Shukla¹, Aditya Vaishya^{6,7}, Lokesh Kumar Sahu⁸, Tim Butler², Narendra Ojha⁸

¹Space Applications Centre, Indian Space Research Organisation, Ahmedabad 380015, India

5 ²Research Institute for Sustainability - Helmholtz Centre Potsdam (RIFS), Potsdam, 14467, Germany

³University of Ladakh, Leh, Ladakh 194101, India

⁴Formerly at University of Ladakh, Leh, Ladakh 194101, India

⁵Rashtriya Raksha University, Leh, Ladakh 194101, India

⁶School of Arts and Sciences, Ahmedabad University, Ahmedabad, 380009, India

10 ⁷The Climate Institute, Ahmedabad University, Ahmedabad, 380009, India

⁸Physical Research Laboratory, Ahmedabad, 380009, India

*Correspondence to: Imran A. Girach (imran.girach@gmail.com) and Sonam Angmo (sonaman36@gmail.com)

Abstract

15 The Trans-Himalaya, located between the Great Himalaya and the Tibetan Plateau, is ecologically fragile and one of the most climate-sensitive regions. However, lack of systematic in-situ measurements have hindered the evaluation of chemistry-climate models and constrained our understanding of the global-to-regional influences over this region. To address this, we present a comprehensive analysis by combining first yearlong (October 2024–September 2025) surface ozone
20 (O₃) measurements at Leh (3.4 km above mean sea level) with satellite data and numerical simulations (global model: CAM4-Chem, regional model: WRF-Chem). Our measurements revealed a noontime O₃ build-up (~3–7 ppbv), a feature typically absent over high altitude mountains. WRF-Chem suggests that this feature is driven by photochemical production (NO_x-VOC transition regime for higher O₃) and entrainment. Despite partial compensation of nighttime loss by noontime build-up, the region acts as a net chemical sink. Seasonal cycle peaks in June (~64±6 ppbv; touching air quality threshold), unlike typical premonsoon peaks over Gangatic and Himalayan regions. CAM4-Chem simulation with CAMS-derived stratospheric contribution, captured the O₃ seasonality, but overestimated the wintertime levels by 10–16 ppbv. Tagged O₃-tracer analysis shows significant contributions of anthropogenic NO_x emissions from South Asia (15–18 %) and other regions (32–37
25 % to O₃ levels. Additionally, stratospheric inputs and biogenic emissions shape the seasonal cycle. This study provides insight into the chemistry and dynamics governing O₃ over the Trans-Himalaya across different time scales. These findings are invaluable for designing future field observations, model improvements, and policy planning for this region.

35 **Keywords:** Ladakh, free-troposphere, stratospheric intrusion, WRF-Chem, CAM-Chem, air quality, atmospheric composition, photochemistry, transport, source attribution



1. Introduction

Tropospheric ozone (O_3) plays a tripartite role: a primary controller of the atmosphere's oxidative capacity, a significant short-lived climate forcer, and a secondary air pollutant (Seinfeld and Pandis, 2016). High levels of ground level O_3 adversely impact human health, vegetation, crop yield and ecosystem (Chuwah et al., 2015; US EPA, 2013). Tropospheric O_3 also acts as a greenhouse gas, produced photochemically by methane (CH_4), carbon monoxide (CO), and non-methane hydrocarbons (NMHCs) in the presence of nitrogen oxides (NO_x). Thus, O_3 is considered an important link between air quality and climate. O_3 has a longer lifetime (6–27 days) in the free troposphere compared to the boundary layer (few hours to ~1 week), due to weaker loss processes associated with lower water vapour and negligible deposition (Prather and Zhu, 2024). Therefore, free-tropospheric O_3 levels can sustain more than those within the urban or rural local boundary layers, and hence such observations would be better representative of regional conditions. In addition, free-tropospheric O_3 variations can provide insights into vertical transport including stratospheric intrusions as well as in situ or en-route O_3 formation through convectively transported precursors (Ansari et al., 2025; Nalam et al., 2025; Ojha et al., 2012; Sahu et al., 2009; Sinha et al., 2016). O_3 mixing ratios generally increase with altitude owing to more intense solar radiation and low concentrations of the titrating gases, for example, NO (Chevalier et al., 2007). The intrusions of O_3 -rich stratospheric air also enhance O_3 levels more at higher altitudes compared to low-altitude plain regions (Cristofanelli et al., 2010). Therefore, studies on ozone variations at high-altitude remote stations are critical to obtain comprehensive insights into the roles of regional emissions, photochemistry, long-range transport, and stratospheric intrusions (Kumar et al., 2010; Sarangi et al., 2014).

Ladakh is a Union Territory (a region directly governed by the central government) and the northernmost part of India, situated in the Trans-Himalayan region between the Karakoram and Great Himalayan ranges. It is one of the coldest, driest and most sparsely populated regions in South Asia and is suggested to be one of the most climate-sensitive, highly vulnerable, and ecologically fragile regions of the world (Goodrich et al., 2019; Wester et al., 2019). Ladakh lies in one of the three subdivisions of Hindu Kush Himalaya (HKH), i.e., north-western Himalaya and Karakoram range (32° – 39° N; 71° – 79° E). The International Centre for Integrated Mountain Development (ICIMOD) have reported that HKH is warming faster than the average rate of global warming with adverse impacts on the cryosphere, hydrology, ecology, vegetation, wildlife, and human society (Nair et al., 2024; Wester et al., 2019). Annual mean temperature has risen by more than 2°C in Leh region over the



70 period of 13 years (1995–2009; Chevuturi et al., 2018). This region is already experiencing
substantial consequences of the climate change, e.g., increased glacier retreating, water scarcity,
heatwaves, landslides, flash floods, debris flows, and soil erosion, etc (Bhattacharjee and Dutta,
2023; Dubey et al., 2025; Khanday et al., 2024; Pandit, 2013; Ziegler et al., 2016). Being a high-
altitude region, remote from major anthropogenic emissions, Ladakh experiences a cleaner
75 background atmospheric conditions, as compared to the densely populated and global hotspot of
emissions—the Indo-Gangetic Plain (IGP) in its immediate south. Due to spatial proximity plus strong
atmospheric dynamics, the transport of trace gases and aerosols from IGP can potentially influence
the Trans-Himalaya also, as observed for the Himalayan region (Das et al., 2022; Hassan et al., 2023;
Ojha et al., 2012; Sarangi et al., 2014). Signatures of aged background aerosols as well as new-
80 particle formation from gaseous precursors suggest a unique chemical environment over Trans-
Himalaya (Ningombam et al., 2014).

Variations in O₃ over the high-altitude Ladakh region can provide invaluable insights into the regional
background, long-range transport, stratospheric intrusions, besides into photochemistry intensified
by higher solar radiation. This region also falls under one of the global hotspots of Stratosphere-
85 Troposphere Exchange (STE; Škerlak et al., 2014). In other words, this region —one among a few
places in the globe (e.g., Mt. Bachelor Observatory, Pico Mountain Observatory; Okamoto and
Tanimoto, 2016), is unique as the amalgamation of regional emission with the influx from free-
troposphere and stratosphere is interacting with intense solar radiation at such a high elevation.
Besides its role in photochemistry and atmospheric dynamics, O₃ monitoring is crucial from an air-
90 quality perspective, as elevated O₃ levels pose significant respiratory risks to populations already
exposed to low oxygen conditions at high altitudes (~3.4 km above mean sea level and higher).
Moreover, even moderate O₃ concentrations can have prolonged ecological impacts on the fragile
ecosystems of the Trans-Himalaya.

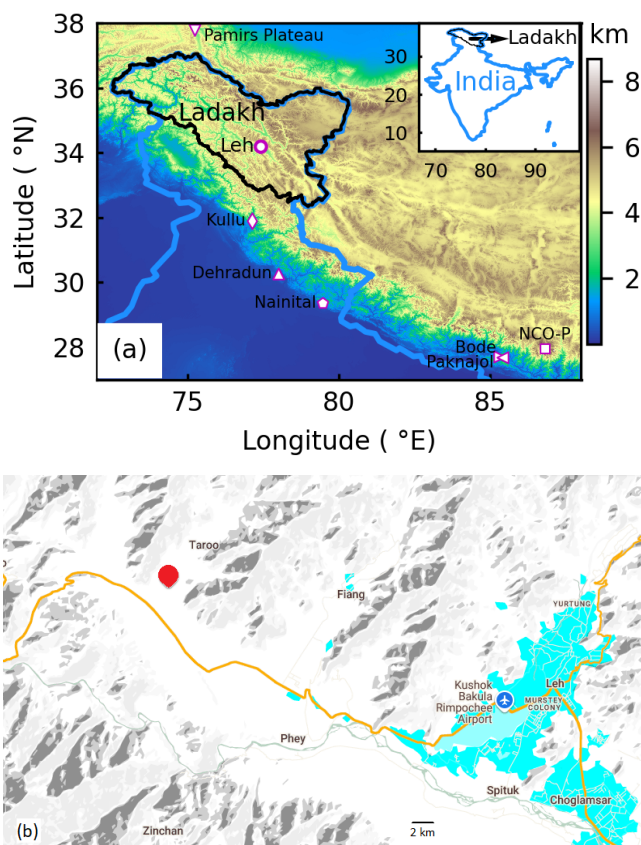
Despite the discussed significance, to the best of our knowledge, comprehensive studies combining
95 systematic in situ measurements, satellite data, and chemistry-transport modeling are lacking over
the Trans-Himalaya. Tourism and urbanization have been increasing in Ladakh particularly since it
became a union territory in October 2019. Therefore, it is timely to initiate studies on air quality and
chemistry-climate processes in this unique environment of the world. In this regard, here, we
present the first detailed investigation into the chemistry and dynamics of O₃ over Ladakh by
100 exploiting the potentials of field measurements, satellite data, and regional and global atmospheric
chemistry-transport modeling.



The remainder of the manuscript is organised in three sections. In section 2, we describe the study region, in situ measurements, satellite data, models, and air quality indices used in the study. In section 3, we present the results and discussion on diurnal variations, daytime O₃ build-up, day-to-day changes, air quality assessment, photochemical regime of O₃ formation, seasonal variation and its drivers, and long-term trends. In section 4, we present the summary and conclusions of our study.

2. Data and methodology

2.1 Study region and in situ measurements



110 Figure 1: (a) Elevation map of the northern Indian Subcontinent. The location of the measurement site (Leh, Ladakh) is marked as a magenta circle. Other nearby sites are also shown which are used for comparison of O₃ variations. Inset in (a) shows a wider view, depicting Ladakh region in northern most part of India. (b) Zoomed map around measurement location, i.e., University of Ladakh (red symbol) and adjacent Leh town (big cyan patch). A highway is shown with an orange curve.



115 Surface O₃ measurements has been carried out since October 2024 at the University of Ladakh
(34.185° N; 77.412° E; ~3.4 km amsl), which is ~16 km (aerial distance) away from the Leh town
(figure 1b; modified from maps.google.com). No major local anthropogenic activity occurs within the
radius of 12–15 km. Temperature, relative humidity, surface pressure and daily accumulated rain
were observed in the range of -10–24 °C, 6–98 %, 651–668 hPa, 0–36.5 mm, respectively at Leh as
120 per the India Meteorology Department. Temporal variations in these meteorological parameters are
shown in figure S1. The synoptic winds at 600 hPa, obtained from the European Centre for Medium-
Range Weather Forecasts (ECMWF) Reanalysis 5 (ERA5; Hersbach et al., 2020), show jumbled winds
(owing to the complex topography) with downdrafts during winter and pre-monsoon. However,
north-westerly or westerly winds prevailed without downdrafts during the monsoon and post-
125 monsoon seasons (figure S2). Further details on the climate of the Leh region are available
elsewhere (e.g., Chevuturi et al., 2018).

In situ O₃ measurements have been carried out using a factory-calibrated (NIST Traceable) ultraviolet
(UV) photometric analyser (2B Tech, USA; Model: 106-L). Air samples were drawn from a height of
~10.6 m above the ground using a Teflon tube through a 5 µm non-reactive polytetrafluoroethylene
130 hydrophobic dust filter. The analyser measures O₃ based on the absorption of UV radiation at ~245
nm applying the Beer–Lambert law. The lower detection limit, linearity, and minimum response time
are 3 ppbv, ±1 %, and 20 s, respectively. The measurement uncertainty of the UV photometric
analyser is reported to be approximately 5 % (Tanimoto et al., 2007). The instrument was
continuously operated in a temperature controlled environment maintaining its permissible limits of
135 temperature (0–50 °C). Inter-comparison of this instrument with a calibrated O₃ analyser (Thermo
Scientific, USA) using a common inlet system showed an excellent agreement (figure S3), prior to its
deployment at the site. Measurements were recorded at an averaging interval of 5 minutes and
were converted to hourly averages for the analysis.

2.2 Satellite observations

140 To interpret the observed O₃ variability and assess long-term changes, the study utilized
tropospheric columns of HCHO and NO₂, along with total column CO, derived from TROPOMI
(TROPOspheric Monitoring Instrument) aboard the polar-orbiting Sentinel-5 Precursor satellite
(equator crossing time: ~13:30 local time). NO₂, HCHO and CO are derived from the spectral
measurements in 405–465 nm, around 2.3 µm and 328–359 nm, respectively. The retrieval
145 algorithms and validations have been described in previous literature (Borsdorff et al., 2018; De
Smedt et al., 2018; Landgraf et al., 2016; Van Geffen et al., 2022). Offline level-3 products of NO₂ and
HCHO are available at spatial resolution of 3.5 × 5.5 km² and CO is available at spatial resolution of



7.5 × 5.5 km² (across × along track) since 28 June 2018. Data with quality assurance greater than or equal to 0.50 (0.75 for NO₂) were obtained from Google Earth Engine, 150 <https://code.earthengine.google.com>.

To consider the possible influences of cloudiness on atmospheric chemistry, we have also utilized data from the Indian geostationary satellite, INSAT-3DS (Indian National Satellite - 3D second repeat). Level-2B cloud mask (L2B CMK) is derived from three infrared channels of the imager (Mid-wave infrared: 3.9 (3.80–4.00) μm, Thermal infrared-1: 10.8 (10.3–11.3) μm, Thermal infrared-2: 12 155 (11.5–12.5) μm) and data is available at 30-minute intervals with a spatial resolution of 4 km. Details of the algorithm can be found here: http://mosdac.gov.in/doc/INSAT_3D_ATBD_MAY_2015.pdf. We considered 25 pixels with a central pixel lying over the study site during the morning hours (8:30–14:00 IST—Indian Standard Time) and summed up the number of cloudy pixels on a daily basis. These daily sum values were used to obtain the monthly averages of the number of cloudy pixels.

160 **2.3 Reanalysis datasets**

Surface O₃ and stratospheric ozone tracer (O₃s) from the Copernicus Atmosphere Monitoring Service (CAMS; Inness et al., 2019), available at 3-hour interval with a spatial resolution of 0.75° × 0.75°, have been used to analyse the seasonal pattern, stratospheric contribution, and long-term trend during the 2015–2024 period. This is the fourth generation ECMWF global reanalysis of atmospheric 165 composition (EAC4). Monthly mean vertical wind from ERA5—ECMWF Reanalysis 5 (hourly interval; 0.25° × 0.25°; Hersbach et al., 2020) is used to understand the prevailing downdraft/updraft. Both CAMS and ERA5 utilise the ECMWF Integrated Forecasting System (IFS) with 4D-var data assimilation. CAMS employs a fully integrated chemistry framework based on the Carbon Bond (CB05) mechanism, comprising 54 species and 126 reactions (Huijnen et al., 2010), with assimilation 170 of satellite observations. Further details of the evaluation of these reanalyses can be found elsewhere (Harithasree et al., 2024; Inness et al., 2019; Park et al., 2020). The CAMS time series at grid, 33.75° N; 78.25° E, closest to the study region is considered for the analysis.

2.4. Global model simulations and source tagging

We have utilized output from dual-source tagging-enabled global model CAM4-Chem (Community 175 Atmosphere Model with Chemistry version-4; Butler et al., 2020) available for a 19-year period of 2000–2018, as described in Ansari et al., (2025) and Nalam et al., (2025). Hourly surface O₃ mixing ratios along with its tagged contributions have been analysed at the grid cell, closest to the observation site. The model calculates O₃ contributions from both NO_x as well as VOC (including CO and CH₄) through two separately tagged simulations. Geographic definitions of specific source



180 regions are shown in figure S4. Monthly varying gridded anthropogenic emissions of NO_x, CO, SO₂, NH₃, OC, BC and NMVOCs, input to the model, are based on the HTAPv3.1 global mosaic inventory for the 2000–2018 period (Crippa et al., 2023). Biogenic emissions are included from the CAMS-GLOB-BIO-v3.0 (Sindelarova et al., 2022) while biogenic soil NO_x is specified as in Tilmes et al. (2015). Biomass burning emissions are prescribed from GFED-v4 inventory (Van Der Werf et al., 2010). The
185 model has a horizontal resolution of 1.9°×2.5°, with 56 vertical levels extending up to model top at approximately 1.86 hPa. The model setup and evaluation results assessing the same global simulations have been discussed in recent studies over North America and Europe (Ansari et al., 2025), East and Southeast Asia (Lu et al., 2025), and the global troposphere (Nalam et al., 2025). In this analysis, stratospheric O₃ contribution to surface O₃ has been considered from CAMS reanalysis
190 as this adjustment improved the agreement of CAM4-Chem simulation with observations. Note that since the latest emissions for 2024–2025 are unavailable, we have used simulation results from previous years, 2009–2018, as climatological mean.

2.5 Regional model simulations

We have performed regional-scale numerical simulations of meteorological parameters and
195 atmospheric composition at spatial resolution of 12 km x 12 km, by applying the Weather Research and Forecasting model coupled with Chemistry (WRF-Chem; Grell et al., 2005; Skamarock et al., 2019) version-4.5.1. Simulations have been conducted for 2 full months, February representing winter and September representing monsoon. Meteorological fields input to the model are based on ERA5 reanalysis (Hersbach et al., 2020). For parametrizing cumulus physics and boundary layer
200 processes, the Grell 3D (Grell and Dévényi, 2002) and Yonsei University (Hong et al., 2006) schemes, respectively, have been utilized. To limit errors in large-scale meteorological and dynamical variations, the temperature, horizontal winds, and water vapour have been nudged at all vertical levels with nudging coefficients of $3 \times 10^{-4} \text{ s}^{-1}$ (Otte, 2008; Sharma et al., 2017).

Anthropogenic emissions are based on the EDGAR (Emissions Database for Global Atmospheric
205 Research) inventory for year 2015 (Crippa et al., 2020; Mogno and Marvin, 2022) and fire emissions are based on FINN v2.5 (Fire INventory from NCAR (National Center for Atmospheric Research); Wiedinmyer et al., 2023) for year 2021. Natural biogenic emissions are computed online using the MEGAN (Model of Emissions of Gases and Aerosols from Nature Guenther et al., 2006). Gas-phase chemistry is represented by the MOZART (Model for Ozone and Related chemical Tracers)
210 mechanism (Emmons et al., 2010) and aerosols are calculated using the MOSAIC (Model for Simulating Aerosol Interactions and Chemistry; Zaveri et al., 2008). Initial and lateral boundary conditions for the chemical fields have been provided from the WACCM (Whole Atmosphere



Community Climate Model) global simulations (Gettelman et al., 2019). We have noted a systematic overestimation of O₃ in remote environments of India and that reducing inflow from the global model by about 40 % leads to better agreement between WRF-Chem output versus measurements. Comparison of model simulated surface O₃ with measured O₃ shows a good agreement (r=0.4–0.8) with smaller negative bias of 6–8 ppbv (figure S5). This shows the model's capability to capture the observed variations reasonably and hence it can be used to gain deeper insights into the various processes contributing to observed variations. The tendency terms in the WRF-Chem (Barth et al., 2012; Girach et al., 2017) have been analysed to quantify roles of various chemical and dynamical processes in influencing O₃ variations. More detailed description of the WRF-Chem model (Grell et al., 2005) and its evaluations and diverse applications over Indian subcontinent can be found elsewhere (Ghude et al., 2025; Girach et al., 2017; Kumar et al., 2012; Sharma et al., 2017).

2.6 Indices for air quality assessment

Maximum Daily 8-h Average ozone (MDA8) is related to short-term health impact with a threshold value of 100 µg m⁻³ set by the World Health Organization (WHO, 2021) as well as by India's National Ambient Air Quality Standards (NAAQS; https://cpcb.nic.in/uploads/National_Ambient_Air_Quality_Standards.pdf; last access: 03 January 2026). MDA8 is a maximum value of 8-h running averages obtained using hourly O₃ on a daily basis. Hourly O₃ mixing ratio (ppbv) is converted to concentration (µg m⁻³) using measured pressure and temperature (figure S1). To quantify health impacts due to long-term O₃ exposure, another metric OSDMA8 (ozone season daily maximum 8 h average) has been estimated, which is basically the annual maximum of six-month running mean of MDA8 (Murray et al., 2020). The risk to vegetation/crops and ecosystems can be assessed based on the estimation of four different metrics: M7 (7-hour Mean, averaged during daytime, 09:00–16:00 h), AOT40 (Accumulated exposure to Ozone above a threshold of 40 ppbv), SUM06 (the sum of all hourly O₃ concentrations ≥0.06 ppm) and W126 (hourly concentrations weighed by a sigmoidal weighting function). AOT40, SUM06 and W126 are calculated for daylight hours, 07:00–18:00 h (Fuhrer et al., 1997; Hogsett et al., 1988; Lee et al., 1988; Lefohn and Runeckles, 1987; Mills et al., 2007). SUM06 and W126 better represent the crop loss as found in the experimental studies in the US (Kaylor et al., 2023). Threshold value or safe limit for AOT40 is 1 ppmv h as defined by UNECE (United Nations Economic Commission for Europe), 1996 (Fuhrer et al., 1997; https://www.umweltbundesamt.de/system/files/medien/4038/dokumente/manual_complete_english.pdf). There are no thresholds defined for M7, W126 and SUM06 as lower levels of O₃ can also have adverse impacts on vegetation. Formulae for these exposure indices are given in supplementary text S1.

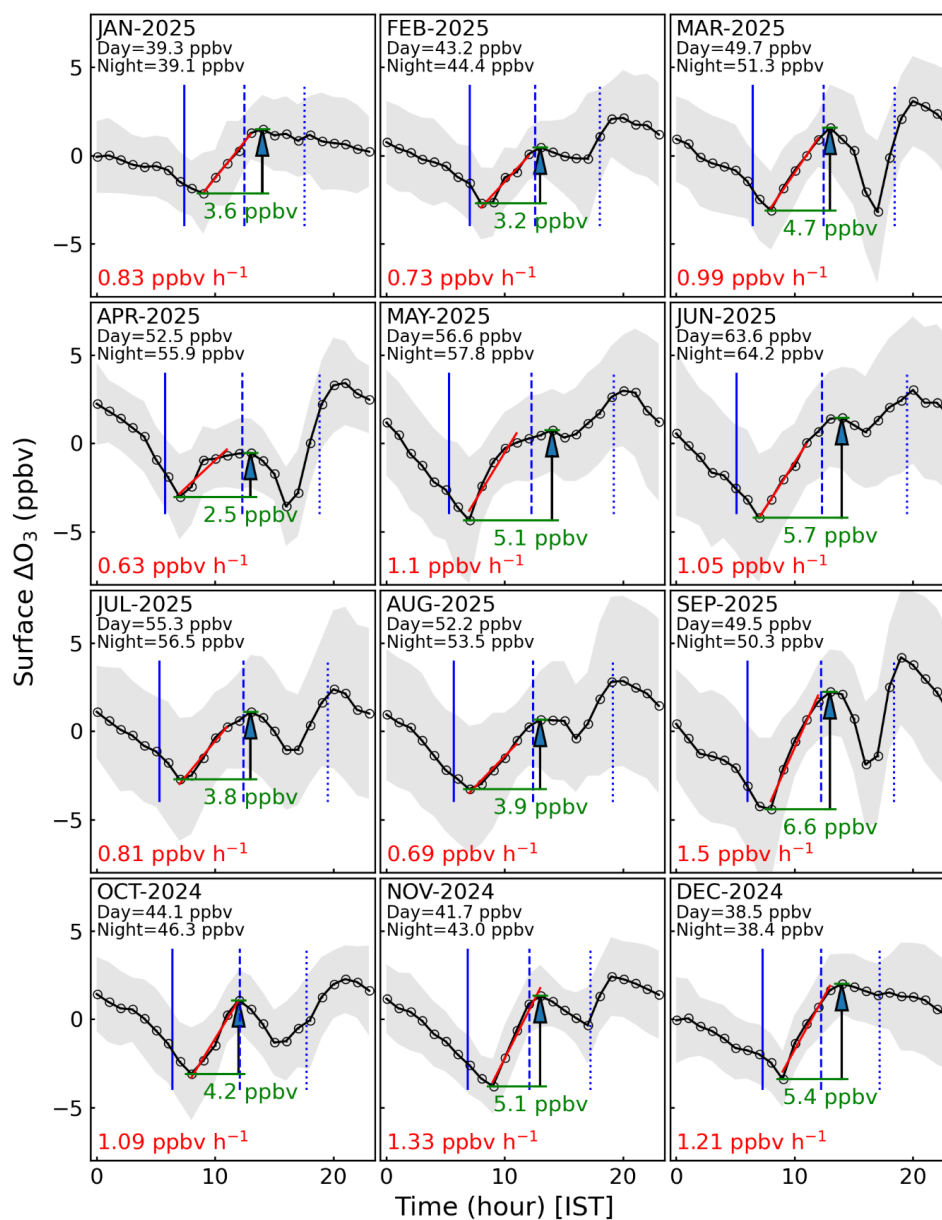


250 3. Results and Discussions

3.1 Diurnal variations and daytime O₃ build-up

ΔO_3 for a given day is obtained by subtracting the daily mean from the hourly values of the corresponding day. The mean diurnal patterns of ΔO_3 for different months are shown in figure 2. The average diurnal variations for different seasons are shown in figure S6. The diurnal patterns of ΔO_3 are observed to be quite unique in this region, nevertheless, similar across different months, with three important features: (a) nighttime (22–7 h) decline, (b) build up after sunrise to the noontime (7–14 h) followed by decline in the afternoon (13–17 h), and (c) increase in the evening (17–20 h). Noontime peak values are comparable or lower than midnight/nighttime values. Since daytime values are generally lower than nighttime values by 0–3 ppbv, there appears to be a net chemical loss on a daily scale. However, to a certain extent, this shows that O₃ loss occurring during nighttime (20–6 h) is partially compensated by daytime photochemical production. The day-to-day variability, as represented by the standard deviation (shaded region in figure 2) is seen to be larger (3–5 ppbv) during monsoon, as compared to other seasons (1–4 ppbv). This is likely due to sporadic mixing of different air masses owing to changes in meteorological conditions, especially day-to-day changes in convection strengths during July to September (Romatschke and Houze, 2011).

The rate of increase from morning (7–9 h) to afternoon (12–14 h) is estimated as the slope of linear fit to five successive hourly values from the morning minimum value, which ranged between 0.6–1.5 ppbv h⁻¹. The photochemical O₃ build-up, estimated as the noontime maximum minus morning minimum, ranged from 2.7–6.6 ppbv. O₃ concentration starts increasing in the morning 1.5–2 h after sunrise. The O₃ curve attains its peak 0–2 h after the local noon (zenith). The evening increase is mostly before sunset (figure 2). Interestingly, the evening O₃ peak is higher than the noontime peak for most of the months, except during winter.

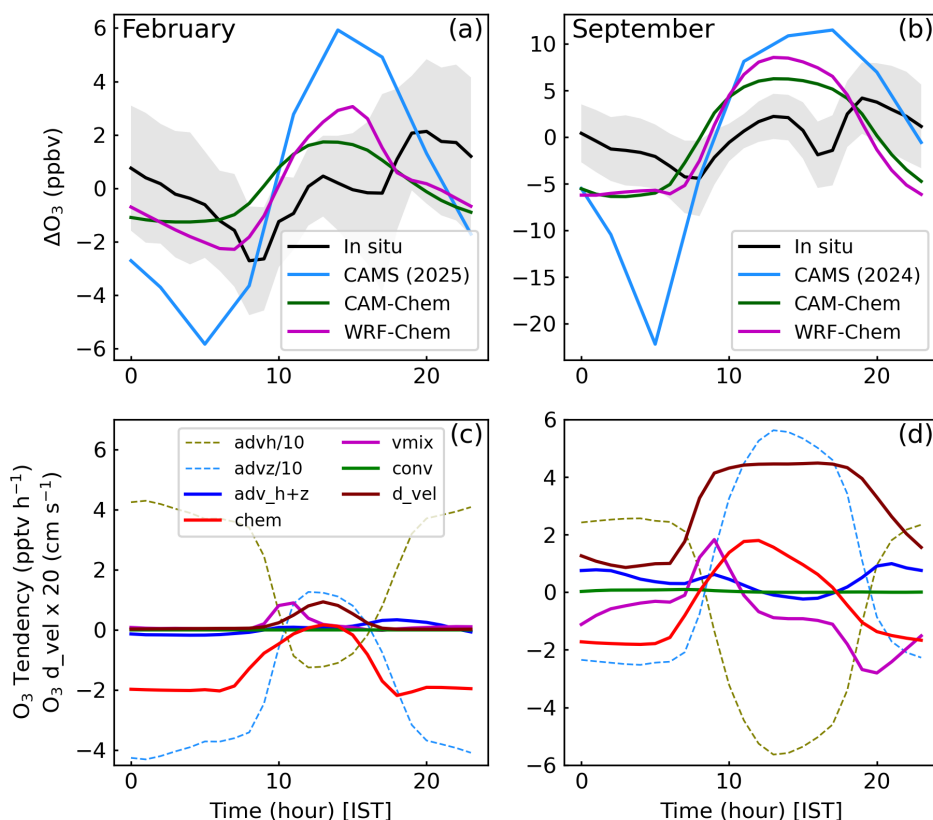


275 Figure 2: Monthly mean diurnal variations of ΔO_3 over the Trans-Himalaya. The shaded grey region shows the standard deviation. The red line shows the linear fit over the 5-h period from the morning minimum. The slope representing net O_3 production rate ($ppbv\ h^{-1}$) is given in red colour font. Total daytime build-up, noontime maximum minus morning minimum, is marked in green colour. Vertical blue lines represent sunrise (continuous line), local noon (dashed line) and sunset (dotted line).



280 Mean values of daytime and nighttime O_3 are also mentioned. Here, daytime is defined as 2 hours
after sunrise until 2 hours before sunset. Likewise, night is defined.

It is important to note that the study region experiences a photochemical O_3 build-up after sunrise, a
feature typically unseen over other high-altitude sites such as Nainital (1.9 km amsl, Sarangi et al.,
2014), Mount Abu (24.6° N, 72.7° E, 1.7 km amsl, Naja, 2003), Mount Fuji (35.4° N, 138.7° E, 3.7 km
285 amsl; Tsutsumi et al., 1994), Ooty (11.4° N, 76.7° E, 2.5 km amsl; Udayasoorian et al., 2013) and
Ponmudi (8.76° N, 77.11° E, 1 km amsl; Ajayakumar et al., 2024). In particular, the ΔO_3 diurnal
patterns show decline after the sunrise or remain nearly stable throughout the day over high-
altitude sites in the Himalaya (Nainital and NCO-P; figure S6). Afternoon time O_3 enhancements at
Nainital was attributed to transport of pollutants from adjoining low-altitude IGP (Indo-Gangetic
290 Plain) through boundary layer mixing. This comparison suggests that unlike the central/eastern
Himalaya, there are significant precursors over the Trans-Himalaya which can result in observed
photochemical O_3 production in the presence of intense solar radiation. Note that due to its higher
elevation, the Trans-Himalaya region receives more intense solar radiation ($7 \text{ kWh m}^{-2} \text{ d}^{-1}$) than
central Himalayas or other lower elevation sites ($5.6 \text{ kWh m}^{-2} \text{ d}^{-1}$) in India (Santra, 2016). Note that
295 here O_3 production rate is slower ($0.6\text{--}1.5 \text{ ppbv h}^{-1}$) than that in polluted valleys and foothills of the
Himalaya ($4.7\text{--}10.1 \text{ ppbv h}^{-1}$; Ojha et al., 2019). For further insight into photochemistry, we analysed
co-located satellite observations to identify O_3 formation regime which are discussed later in section
3.4.



300 Figure 3: (a–b) Comparison of observed diurnal ΔO_3 variation at Leh with simulations from global (CAM5 and CAM-Chem) and regional (WRF-Chem) models. WRF-Chem inferred deposition velocity (d_{vel}) and mean tendencies due to different processes: horizontal advection (advh), vertical advection (advz), convection (conv), chemistry (chem), and vertical mixing (vmix) are shown in (c–d).

Qualitatively, the models reproduce the diurnal ΔO_3 pattern, except missing the late evening-time enhancement. Quantitatively, diurnal amplitude in CAM4-Chem as well as WRF-Chem models matches with the observations (~ 3 ppbv) during February. Both models do show an increase in diurnal amplitude in September but overestimate its magnitude (12–15 ppbv) than observed values (7 ppbv). However, chemistry appears much more intense in the CAM5 reanalysis particularly during September. Our results suggest that simulations from CAM4-Chem and WRF-Chem may be analysed for deriving further insights into the factors governing O_3 magnitude and variations. Few other limitations which we are reporting here, although are not quite surprising, would be useful for future improvements and fine-tuning of the models. It is likely that the evening surge is associated with mesoscale dynamics, transport of O_3 rich air from higher altitudes due to mountain-valley circulation



(Sarangi et al., 2014) or through other orographic influences unresolved even at high resolutions
315 (Singh et al., 2021) in complex Himalayas.

The tendency terms from WRF-Chem simulations have been analysed to infer the main processes governing O_3 diurnal variation during two contrasting seasons (figure 3c–d). The daytime build-up during winter is linked with decreased photochemical loss and increased contribution through vertical mixing in the morning hours (figure 3c). Small contributions from the advection are seen in
320 the evening hours. Contrary to winter, larger photochemical production drives daytime increase of O_3 during monsoon season (figure 3d). Interestingly, while vertical mixing positively contributes to enhanced O_3 in the morning hours, it reduces O_3 in the evening hours in the model. Positive advective contributions help to sustain O_3 levels during the monsoon throughout the day, except near noontime. The deposition velocity of O_3 is elevated during daytime, especially in the monsoon,
325 but it is negligible during nighttime in both seasons. The results suggest higher depositional loss of O_3 in summer as compared to the winter. A slow decrease during nighttime is due to chemical loss plus vertical mixing as seen by negative chemical tendencies during both seasons (figure 3c–d). Thus, the model fields provided key insights into the relative roles of different processes shaping O_3 diurnal pattern, besides indicating the factors that may need improvements to reduce the model-
330 measurement differences such as in late evening or night.

3.2 Day-to-day variations and contributing processes

The day-to-day changes in noontime (13 h) values of O_3 and different tendency terms, as derived from the WRF-Chem simulation, are shown in figure 4. For this, change in O_3 is obtained by subtracting values at 13 h on $(n - 1)^{th}$ day from value at the same time on n^{th} day. Similarly,
335 tendencies shown here are obtained the same way from WRF-chem simulated accumulated tendencies. To assess the role of different tendencies in changing O_3 , correlation coefficient and normalised covariance are also estimated between tendencies versus O_3 change as mentioned in the figure. Day-to-day changes in noontime O_3 are smaller in February (up to 10 ppbv d^{-1}) compared to September (up to 20 ppbv d^{-1}), as seen in figures 4b and i. Chemical tendencies are typically negative
340 over this region (figure 3d, k), being -30 to -40 ppbv d^{-1} in February but 0 to -10 ppbv d^{-1} in September (except during convective episode; 8-11 September). This indicates that the region acts as a net chemical sink of O_3 during both the seasons, being a stronger sink during the winter season. The gradual nighttime (20–6 h IST) declines seen in the observations (figure 2) also support the role of titration of O_3 . Monthly sum of hourly changes in observed O_3 turns out to be negative during most
345 of the months, except in January, March, June, and August (figure S7). This is consistent with the model-based inference that the region acts as a net chemical sink. Dynamics (convection plus



advection) compensated more than the stronger chemical losses during 8–10 September, leading to overall O₃ increase. Little variations in chemical losses in other days but strong anti-correlation in this period led to an overall negative correlation between chemical tendencies and O₃ change in 350 September.

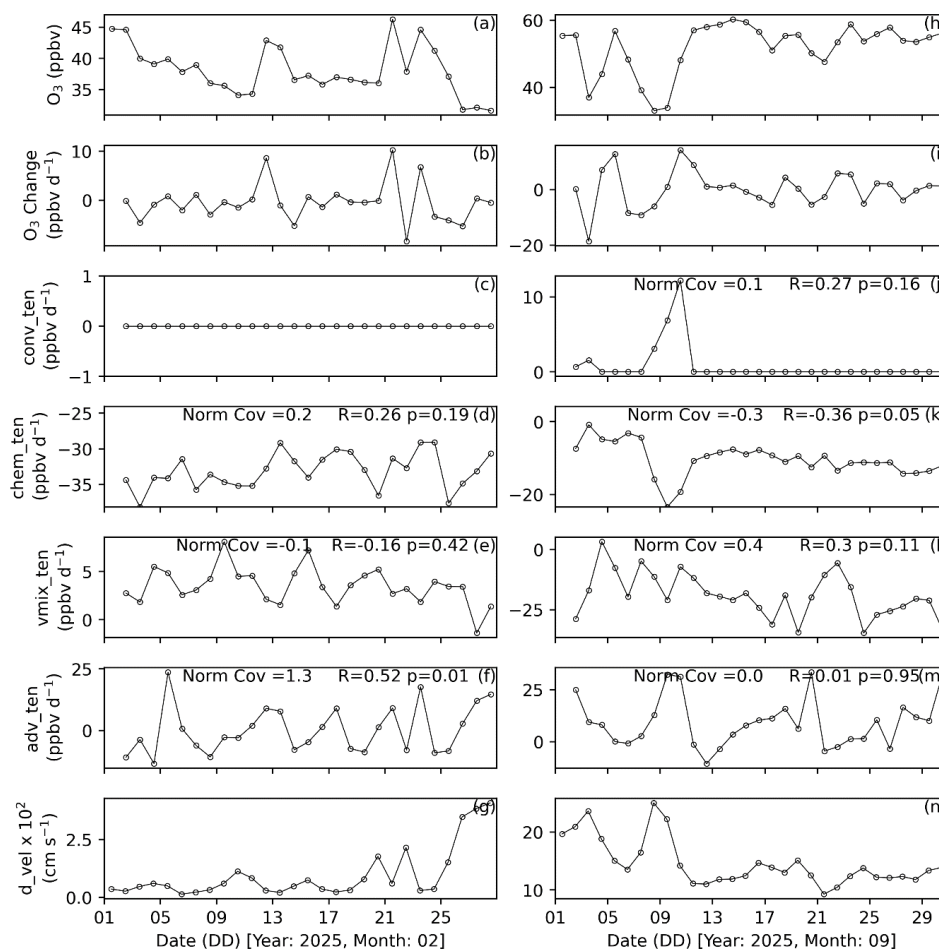


Figure 4: Noontime O₃ (13 h IST), its changes with respect to the previous day, various tendencies and deposition velocity during representative months of winter (a–g) and summer monsoon (h–n) seasons. The y-axis labels, conv_ten, chem_ten, vmix_ten, adv_ten, and d_vel, represent O₃ tendencies (ppbv d⁻¹) due to convection, chemistry, vertical mixing, advection, and O₃ deposition velocity (cm s⁻¹). Correlation coefficient (R) and normalised covariance are between O₃ change (ppbv d⁻¹; b and i) and tendencies (c–f, j–m). Here, covariance is normalised with respect to variance in O₃ change (b and i). The p-value is also marked along with R.



The advection tendencies are generally positive and cause an increase in O_3 . Transport due to
360 advection has a greater bearing on O_3 change during winter, as inferred from the higher correlation
and covariance (figure 4f; $R=0.5$, normalised covariance 1.3). In contrast, no single process
dominates day-to-day O_3 changes during monsoon. The contributions from multiple processes
govern the O_3 changes during monsoon.

Convection is not a key factor in general, except during a large increase in O_3 during 8–11 September
365 when it exceeded 10 ppbv d^{-1} (figure 4c, j). Deposition velocity also shows significant variations
(February: $0.01 \pm 0.01 \text{ cm s}^{-1}$; September: $0.15 \pm 0.04 \text{ cm s}^{-1}$) with enhancements during convective
episodes (e.g., around 9 September 2025).

3.3 Air quality impacts

Our first systematic O_3 measurements can provide insights into O_3 impacts on the public health and
370 vegetation over the Leh region. In this regard, several standard and widely applied exposure metrics
have been estimated and compared with the thresholds (figure 5). All O_3 exposure indices are
observed to be higher during May–July, peaking in the month of June. MDA8 values ranged from 50–
101 $\mu\text{g m}^{-3}$ (36–78 ppbv) during the study period. MDA8 values are very close to the threshold of 100
 $\mu\text{g m}^{-3}$, with 28 days experiencing values above 90 $\mu\text{g m}^{-3}$ and once exceeding the threshold during
375 May–July. OSDMA8 is 80 $\mu\text{g m}^{-3}$ (or 60 ppbv), which is significantly higher than the minimum risk
level of 32.4 ppbv (Turnock et al., 2025). The AOT40 values are above the threshold of 1 ppmv h
except during November–February. Annual cumulative values of AOT40, SUM06 and W126 are
estimated to be 40.7, 37.1, and 36.1 ppmv h, respectively. Magnitudes of these indices are
comparable with those over the US and South Korea (Kaylor et al., 2023; Lee et al., 2023). AOT40,
380 SUM06 and W126 have been reported to range between 0–5, 1–20, and 1–15 ppmv h, respectively,
over China during the crop growing season of winter (Jiao et al., 2025), which are comparable or
slightly higher than the present study region. Increase in AOT40 between 13 to 17 ppmv h is also
reported over the Indian region during wheat growing season (January–March) of 2005–2021
(Anagha and Kuttippurath, 2026). With increasing global baseline O_3 and anthropogenic emissions
385 across South Asia, our results indicate likelihood of more frequent exceedance of air quality
standards in this region. In this regard, O_3 formation regime (Section 3.4) and long-term trends
(Section 3.7) have been analysed for informing the policies.

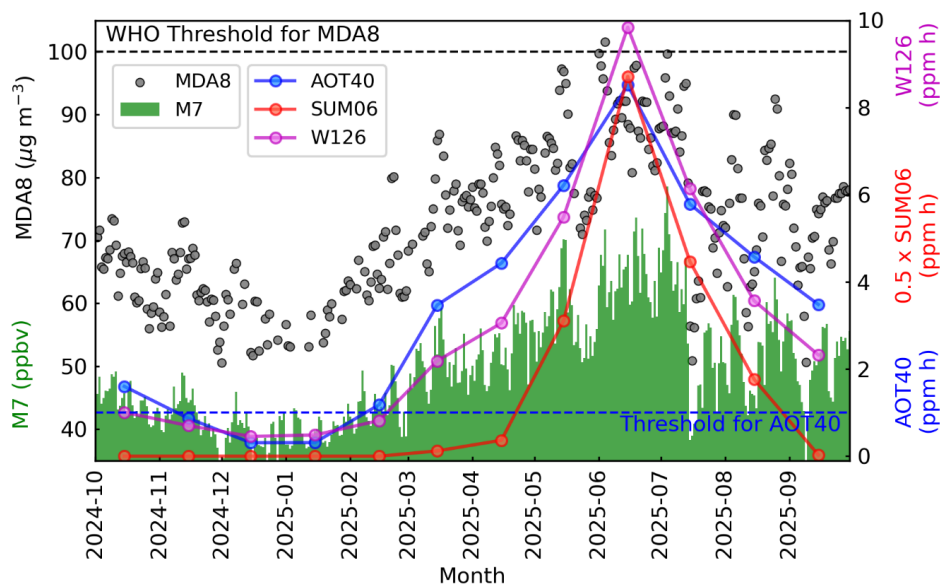


Figure 5: Variations in various ozone exposure metrics during the study period. Threshold values of MDA8 ($100 \mu\text{g m}^{-3}$) and AOT40 (1 ppm h) are indicated by horizontal dashed lines.

3.4 O₃ formation regime

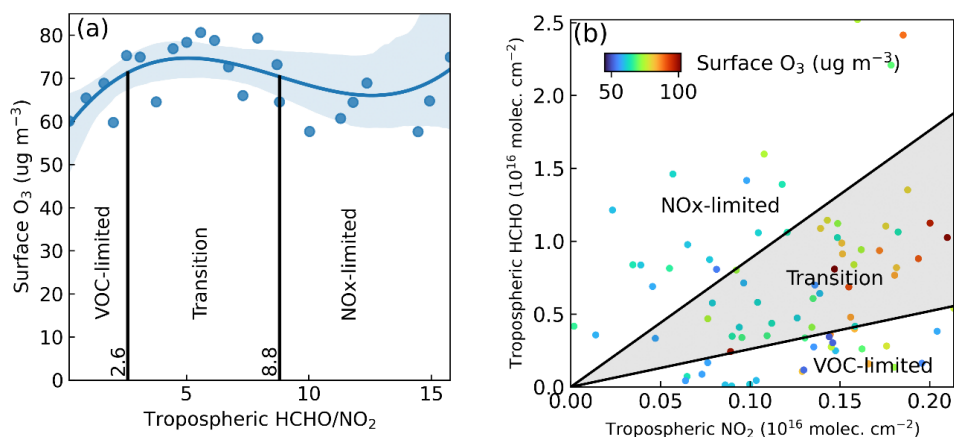


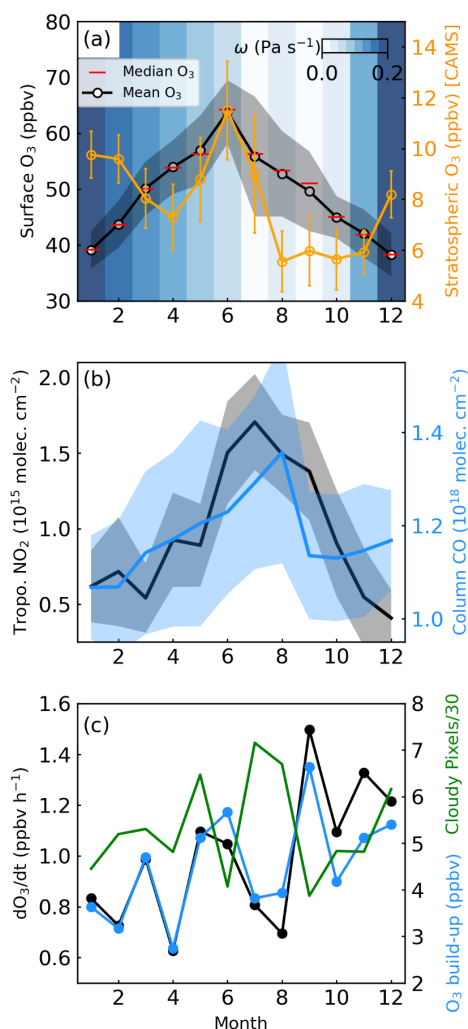
Figure 6: (a) Variations of surface O₃ with collocated tropospheric HCHO/NO₂ ratio over the study region. Blue curve represents the 3rd order polynomial fit with 95 % confidence level (shaded region). (b) Scatterplot of tropospheric HCHO versus NO₂ colour-coded with surface O₃. Black lines in (a) and (b) demarcate O₃ formation regimes, as labelled.



TROPOMI observations of tropospheric HCHO and NO₂ have been used to determine the threshold values of the HCHO/NO₂ ratio to demarcate NO_x and VOC-limited regimes suitable for the study region, following the literature (Jin et al., 2017; Martin et al., 2004). Surface O₃ values are averaged
400 over a ±15-minute time window with respect to the satellite overpass (i.e., 30 minutes centred on the overpass time). The HCHO/NO₂ ratio is divided into 400 bins, and corresponding averages of O₃ are fitted with a 3rd order polynomial as shown in figure 6a. Since the peak of the fitted curve is the central value in the transition regime, i.e., ridge of O₃ isopleths, a slope from -3 to +3 of the fitted curve demarcates the VOC-limited versus NO_x-limited regimes (Ren et al., 2022), corresponding to
405 HCHO/NO₂ ratios of 2.6 and 8.8, respectively (figure 6a). Therefore, the values less than 2.6 represent a VOC-limited regime, whereas the values higher than 8.8 represent NO_x-limited regime. Most of the higher values of O₃ lie in the transition regime (figure 6b) suggesting that the O₃ formation corresponding to higher values is contributed by both NO_x and VOCs and hence the effective mitigation will require reductions in both NO_x and VOCs. In addition, since the O₃ levels are
410 particularly higher during May–July (figure 5), when NO₂/CO ratio suggests prevalence of “relatively” fresh airmasses (compared to winter season; see figure S8), reduction in regional emissions in addition to local emissions would be essential to contain the O₃ level within safe limits.

3.5 Seasonal variation: role of stratospheric intrusion and photochemistry

Figure 7 shows the seasonal variations of observed O₃ and related parameters derived from
415 reanalysis and satellite observations over the study region. O₃ levels are lower during winter (38.3±3.8 ppbv in December), increase in spring and attain maximum in June, just before the summer monsoon (63.8±5.6 ppbv). Note that since summer monsoon onset is late, July rather than June, here monsoon period is from July to September (Bhan et al., 2015). The amplitude of the observed O₃ seasonal cycle is 25.5 ppbv. CAMS derived O₃s climatology shows its peak (11.4 ppbv)
420 during June explaining about 18 % of the seasonal maximum of O₃ over this region (figure 7a). This result is broadly consistent with more stratospheric intrusions over the Tibetan Plateau in the month of June (Liao et al., 2025). The stratospheric contribution is also substantial in winter (8–10 ppbv) but lower during other seasons (5–6 ppbv). Vertical wind at 650 hPa (close to the observed surface pressure of 651–668 hPa; figure S1) from ERA5 shows that the study region experiences downdraft consistently, except during the monsoon (see background colours in figure 7a). Strong downdrafts during winter with higher potential vorticity (5–10×10⁻⁶ K kg⁻¹ m² s⁻¹; figure S9) provide conducive conditions for downward transport of O₃-rich air, in line with the analysis of CAMS O₃s. During June 2025 when O₃ peaked, potential vorticity remained above 2×10⁻⁶ K kg⁻¹ m² s⁻¹ suggesting the presence of stratospheric influence.



430

Figure 7: Seasonal variation in (a) Observed O₃, vertical wind, and stratospheric O₃ tracer (O_{3s}), (b) satellite-derived tropospheric column NO₂ and total CO column, and (c) observed rate of O₃ increase (dO₃/dt), daytime O₃ build-up, and number of cloudy pixels derived from INSAT-3DS (8:30–14:00 IST) over the Leh region. All parameters are for the measurement period (October 2024–September 2025), except O_{3s} for which climatology (2015–2024) is shown. The shaded region in (b) shows the standard deviation.

435

Tropospheric NO₂ and total CO columns from TROPOMI over the study region show higher values (NO₂: 1.4–1.7×10¹⁵ molecules cm⁻²; CO: 1.2–1.4×10¹⁸ molecules cm⁻²) during monsoon (figure 7b).



440 NO₂/CO ratio peaks during June-July (figure S8) suggesting presence of photochemically “fresh”
 airmass likely transported from nearby regions, besides local emissions. The tourist activities are
 generally higher during summer (May–September) peaking in June, as compared to winter (Dolma,
 2020). Larger abundances of the precursors in presence of intense solar radiation provide conducive
 conditions for photochemical O₃ production during June. Figure 7c shows that higher rate of increase
 445 in O₃ (dO₃/dt: 1–1.5 ppbv h⁻¹) and O₃ build-up (5.5–7 ppbv) during June and September but lower
 values during July-August (0.7–0.8 ppbv h⁻¹; ~ 4 ppbv) despite availability of precursors (figure 7b).
 The average number of cloudy pixels during morning hours (8:30–14:00 IST) obtained from INSAT-
 3DS shows more frequent cloudy conditions during July-August, which suppress the photochemistry
 leading to weaker noontime build-up. In addition, rain events during July-August (figure S1) would
 450 have washed out the precursors, inhibiting the O₃ production.

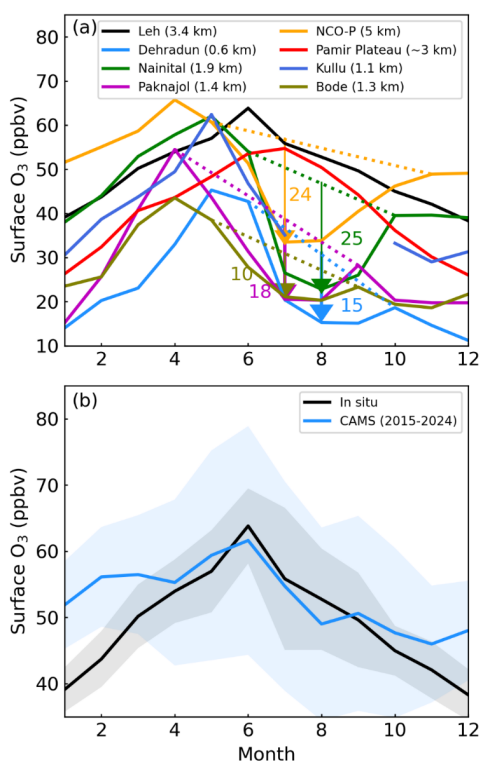


Figure 8: (a) Comparison of O₃ seasonal cycle over Leh with observations in the Himalaya, its foothills and Pamir Plateau. The altitudes of the sites are shown in the legend. Numbers in different colours show the approximate drop in O₃ concentration during monsoon with respect to the hypothetical



455 reference curve (dotted line) connecting pre- and post-monsoon values. (b) Seasonal variation of O₃
460 from measurements and CAMS reanalysis over the study region.

O₃ seasonal variation observed at Leh is compared with those at seven stations across Himalaya (Kullu, Dehradun, Nainital, Paknajol, Bode, NCO-P, and Pamir Plateau), as shown in figure 8a. Monthly mean values are adopted from the literature (Cristofanelli et al., 2010; Harithasree et al., 2024; Mahata et al., 2018; Putero et al., 2015; Sarangi et al., 2014; Sharma et al., 2013; Yongde and Xinchun, 2025). O₃ at Leh peaks in June, unlike other Himalayan sites where it peaks during pre-monsoon season (April-May) except over the Pamir Plateau (Yongde and Xinchun, 2025). Similar to the aforementioned regions, the pre-monsoon peak is ubiquitous in the Gangatic region or northern Indian subcontinent, owing to the regional pollution and intense solar radiation (Lal et al., 2017; 465 Ojha et al., 2022). It is important to note that central Himalaya and its foothills are influenced by transport of precursors from the IGP during pre-monsoon, causing a peak in the seasonal pattern (Kumar et al., 2010; Sarangi et al., 2014). The O₃ level reduces by a large magnitude of 10–25 ppbv during summer monsoon, with reference to pre- and post-monsoon values (dotted line in figure 8a), over most of the sites. This influence of the monsoon is absent over Leh as well as Pamir Plateau. In 470 addition to the difference in the timing of the seasonal peak, the absence of strong monsoonal reduction is another key feature of the Trans-Himalaya.

Figure 8b shows the monthly mean variations of observed O₃ concentrations during 2024–2015 against the climatological mean O₃ (2015–2024) derived from CAMS reanalysis for the study region. The CAMS-derived seasonal climatology agrees well with the observations except during winter. We 475 do not have further parameters from the reanalysis for a deeper analysis of various contributing factors. To find the contributing factors responsible for the observed O₃ variation, we analysed the results from the global chemistry-climate model as discussed in the following section.

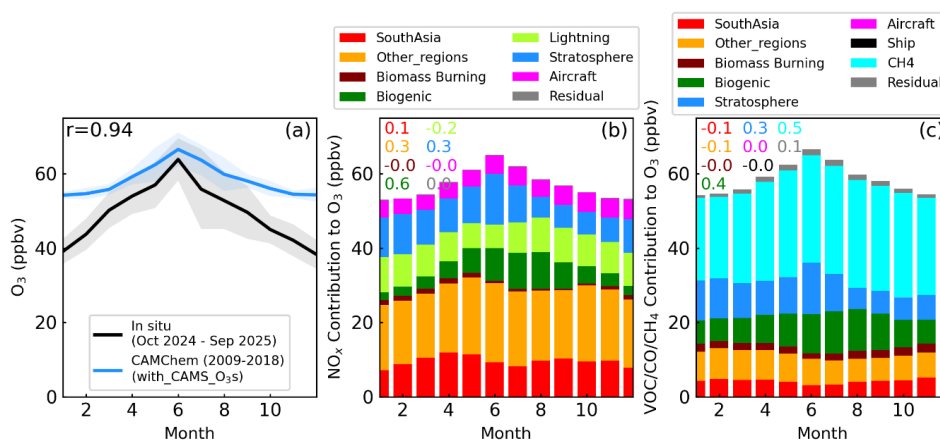
3.6 Source attribution inferred from global model simulations

Figure 9 shows the observed and CAM-Chem simulated seasonal variation of O₃ concentrations over 480 the Trans-Himalaya. The model broadly captures the seasonal pattern ($r=0.94$) with a positive bias of 3–16 ppbv. The lowest bias is seen during the seasonal peak in June. Winter time overestimation (here, 10–16 ppbv) is commonly seen in most of the global models (Ansari et al., 2025; Gao et al., 2025 and references therein), including CAMS (figure 8b). A winter-time positive bias has also been reported for other regions in previous studies (Liu et al., 2022; Miyazaki et al., 2025). This high bias 485 could be attributed to factors such as the inappropriate representation of temperature-dependent chemical and physical processes, and photolysis rates impacted by clouds. Unresolved topography could also contribute to bias as air masses are trapped in the shallow boundary layer during winter



and the associated dynamics may not be captured at the coarse resolutions of the model. A recent study (Wild and Ryan, 2026) used an ensemble of atmospheric model runs with perturbed process parameters and found that the photochemical kinetic parameters and deposition rates, particularly over water and unvegetated surfaces (which largely define our study region), have been the largest source of uncertainty in simulating surface O₃ (Emmerichs et al., 2021). More detailed investigations, especially model intercomparison exercises with perturbed process parameters, and not only with perturbed emissions, are required to pinpoint the causes of model biases (Carslaw et al., 2025).

495



500

Figure 9: (a) Seasonal variations of surface O₃ from in situ measurements and from CAM4-Chem derived climatology (2009–2018) with stratospheric contribution updated by CAMS O₃s, and CAM4-Chem derived contributions to O₃ from (b) NO_x sources and (c) VOC/CO/CH₄ sources. Covariances of different sources normalised with variance in modelled O₃ are marked with respective colours as in the legends in (b) and (c). The shaded region in (a) shows the standard deviations. Note that stratosphere in (b) and (c) refer to stratospheric O₃, rather than contribution from stratospheric NO_x or other precursors.

505

O₃ contributions are highly distributed across diverse NO_x sources: global anthropogenic, South Asian, biomass burning, biogenic, lightning, and stratospheric O₃, highlighting the background characteristic of this region. Interestingly, based on the NO_x tagging (figure 9b), the largest contribution to O₃ in CAM4-Chem model is seen from the anthropogenic sources outside the South Asia (figure S4), accounting for 30.9–36.6 % (17.1–21.3 ppbv). Other major contributions were from anthropogenic NO_x emitted in South Asia (12.9–20.1 %; 7.1–11.9 ppbv), lightning (9.5–17.3 %; 6.3–9.4 ppb), and stratospheric intrusion (9.4–20.7 %; 5.6–13.8 ppbv). Smaller contributors were global aircraft NO_x emission (7.1–9.8 %; 3.9–5.3 ppbv), biogenic emissions from vegetation (3.9–16.3 %;

510



2.1–9.8 ppbv), and biomass burning (0.8–2.6 %; 0.5–1.4 ppbv). Note that the O₃ contribution from global shipping NO_x is included here in the “other regions” segment. The residual is estimated to be negligible (0.14–0.19 ppbv).

Based on VOC/CO/CH₄ tagging (figure 9c), largest contribution of 40.1–50.3 % (21.9–21.2 ppbv) is
515 from oxidation of CH₄, followed by biogenic (11.3–19.0 %; 6.2–11.4 ppbv), anthropogenic NMVOC
emissions from foreign regions outside South Asia (10.3–14.9 %; 6.0–8.1 ppbv), stratospheric
intrusion (9.4–20.7 %; 5.6–13.8 ppbv). Minor contributors were South Asian anthropogenic NMVOC
emissions (4.8–9.5 %; 3.1–5.1 ppbv), and biomass burning (2.3–4.4 %; 1.6–2.4). The contribution of
VOC emissions from aircrafts and ships is negligible (<0.03 ppbv) and the residual is small, 1.4–2.5 %
520 (0.8–1.5 ppbv). Season-wise contributions from various factors are shown as pie charts in figure S10.
Among these different sources, the O₃ contributions from CH₄ oxidation, from biogenic emissions,
stratospheric contribution, and from anthropogenic NO_x emissions outside South Asia show larger
variations (covariance normalised with variance of O₃: 0.3–0.6; see coloured text in figure 10b–c),
and hence these four contributors largely shape the observed seasonal O₃ pattern. While
525 stratospheric intrusion in June, 20.7 % (13.8 ppbv), largely drives the peak in O₃, biogenic emissions
help in maintaining O₃ levels during the monsoon season. In other words, global anthropogenic
influences plus contributions of natural sources (biogenic + stratospheric intrusion) in conjunction
with distinct meteorology of the region sustain substantial O₃ even during the monsoon, a quite
unique feature in South Asia (figure 8a). Since the model show larger bias during winter,
530 interpretations of source attributions needs to be made cautiously.

3.7 Long-term trend in O₃ and its precursors

We have analysed CAM4-Chem long-term simulations to know how O₃ and its sources have changed
over the study region for 1.5 decades, during 2003–2018. Figure 10 shows a time series of de-
seasonalised O₃ and contributions to O₃ from most of the sources as discussed in the previous
535 section. The minor contributors to the study regions (i.e., biomass burning and VOCs from ships) are
not shown here. Here, de-seasonalisation is carried out by removing the mean seasonal cycle from
monthly average values. Linear regression is shown where the trend is statistically significant
($p < 0.01$). O₃ increased over the study region until 2013 with a rate of 0.6 ppbv y⁻¹ and slightly
declined afterwards and the trend is statistically insignificant for the period of 2014–2018 (figure
540 10a). The increasing trend during 2003–2013 is attributed to increasing contributions from NO_x from
South Asia (0.19 ppbv y⁻¹) and outside South Asia (0.23 ppbv y⁻¹), VOC+CO from South Asia (0.11 ppbv
y⁻¹), CH₄ (0.17 ppbv y⁻¹) and stratospheric O₃ (0.31 ppbv y⁻¹). These increasing contributions were
partially offset by a small declining contribution from biogenic NO_x (-0.08 ppbv y⁻¹) during 2003–



2013. The increase and decrease in NO_x contributions from the regions outside South Asia before
545 and after 2013 are due to increasing NO_x emission in the northern hemisphere until 2013 and decline
afterwards (Ansari et al., 2025; Lu et al., 2025). Interestingly, stratospheric O_3 also showed a decline
during 2014–2018, which is unexpected and needs separate investigations. Thus, slight decline or
stationary levels of O_3 during 2014–2018 is due to counterbalance between increasing trend in NO_x
and $\text{VOC}+\text{CO}$ over South Asia and aircraft NO_x emissions; and decreasing trend in NO_x emissions
550 outside South Asia and stratospheric contributions.

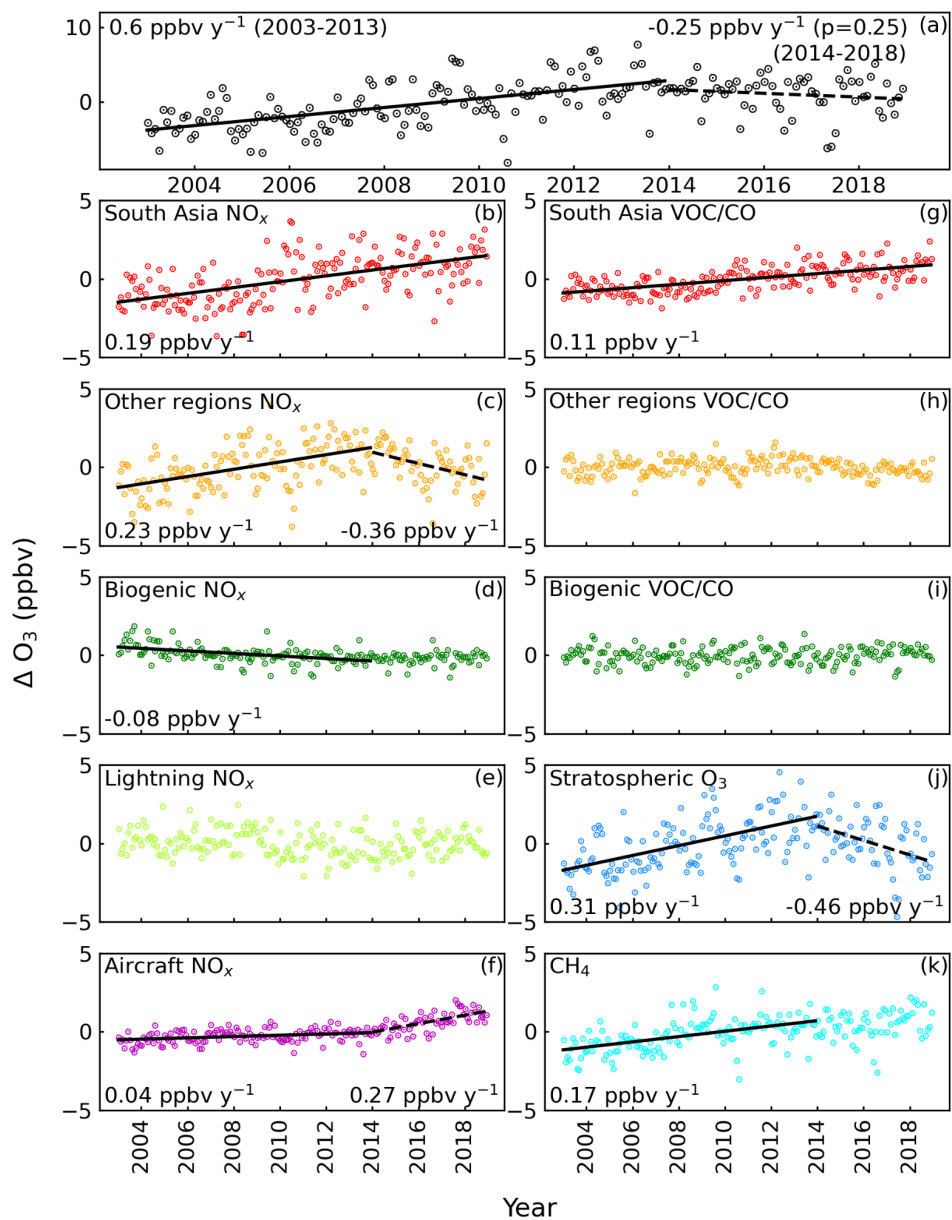


Figure 10: Time series of CAM4-Chem simulated de-seasonalised O_3 (ΔO_3) and contributions from its sources NO_x and $VOC/CO/CH_4$ as labelled in each panel during 2003–2018. Black lines show linear regressions and corresponding trend values are shown in respective panels for 2003–2013 (continuous line) and 2014–2018 (dashed line). All trends are statistically significant (p -value < 0.01),



except for a trend in O₃ during 2014–2018 shown in panel (a). Colours of the scatters are chosen the same as in the figure 9b and c.

In view of the significantly higher values of O₃, nearing air quality thresholds (section 3.3), we have also analyzed the long-term trend in surface O₃ (from CAMS reanalysis) and precursors (from TROPOMI considering region: 77.41°–77.70° E; 34.08°–34.23° N) during the past few years, as shown in figure 11. CAMS O₃ shows a positive trend of 0.69 ppbv yr⁻¹ (1.4 % y⁻¹ with respect to an annual mean level of 50.6 ppbv during 2015). This trend value is larger than previously reported trend over the Indian region at a similar vertical level (0.1 ppbv y⁻¹ during 1994-2019; Gaudel et al., 2024). The magnitude of the trend over the study region is also higher as compared to the observations of surface O₃, 0.1–0.4 ppbv y⁻¹ (1973–2014) at Thiruvananthapuram (8.5° N; 77.9° E, Nair et al., 2018). Trend at 600 hPa over three locations in India (Thiruvananthapuram, Delhi and Pune) ranged -0.1 to 2.3 % y⁻¹ during 1989–2001 (Saraf and Beig, 2004). If only June values of CAMS O₃ are considered where it closely matches with observations, an increasing trend of 0.74 ppbv y⁻¹ is found, which is however statistically insignificant during 2015–2024.

Satellite-derived NO₂ and HCHO, show statistically significant trends of 0.45×10^{14} molecules cm⁻² y⁻¹ (~7 % y⁻¹ with respect to annual mean 6.44×10^{15} molecules cm⁻² for year 2019) and 0.15×10^{15} molecules cm⁻² y⁻¹ (~4 % y⁻¹ with respect to annual mean 6.44×10^{15} molecules cm⁻² for year 2019), respectively, during 2018–2025 (figure 11b and c). However, since the rate of increase in NO₂ is much higher than HCHO, the HCHO/NO₂ ratio is declining at the rate of 0.03 y⁻¹ (figure S11), leading to a reduction from 0.65 in 2019 to 0.45 in 2025. This decline is pushing the O₃ formation regime towards the VOC-limited regime. If this scenario or trend continues further, local production of O₃ is expected to reduce over Leh according to figure 6a, however, regional contribution through transport would decide the net increase/decrease scenario. The observed increase in NO₂ could be partly attributed to the recent increase in the tourism activities in the region. CO does not show consistent increase or decline over the study region (figure 11d), and since it has a longer lifetime of a week to 2 months, the regional variation of CO needs to be investigated further.

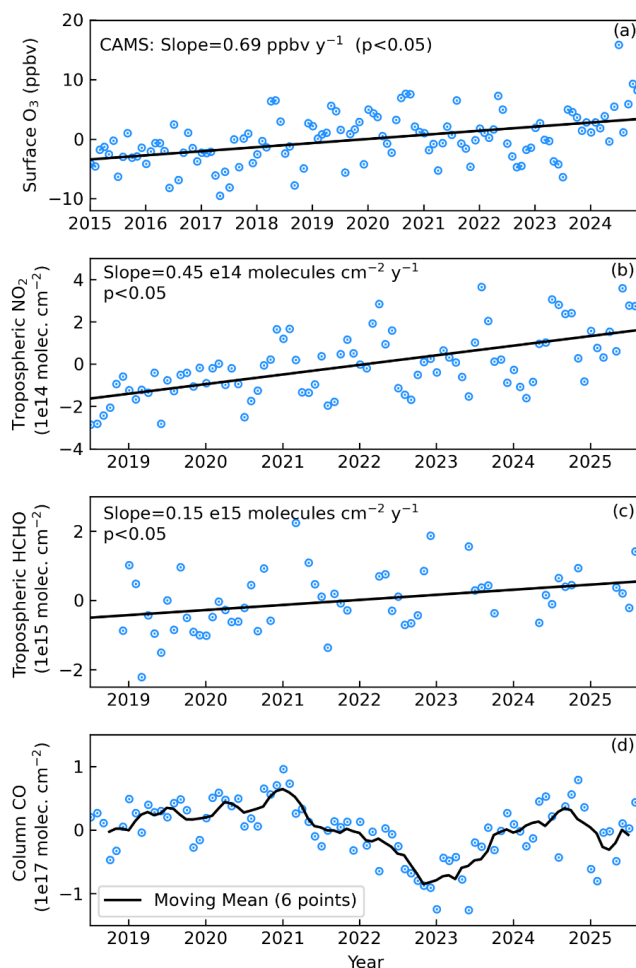


Figure 11: Long-term trend in de-seasonalised monthly mean surface O₃ from reanalyses (2015–2025) and tropospheric NO₂, HCHO and column CO from TROPOMI (2018–2025) over the study region. Trend magnitude, i.e., slope of linear fit, is marked in the top-left corner along with p-value.

4. Summary and conclusions

The dynamics of surface O₃ over the Trans-Himalayan region has been comprehensively investigated for the first time by combining year-long in situ measurements, analysis of satellite observations, and results from global and regional models. The key findings are summarised as follows.

- 590
- Trans-Himalaya is observed to be a unique environment exhibiting a daytime O₃ build-up of 2.7–6.6 ppbv (with rate of 0.6–1.5 ppbv h⁻¹), a feature not observed at high-altitude mountain regions. Despite a daytime build-up partially offsetting the nighttime losses, the region remains



- a net chemical sink. While photochemistry and vertical entrainment are major drivers of diurnal pattern during winter, advection is an additional contributor during monsoon season.
- 595 ● WRF-Chem-derived tendencies suggest that advection is largely responsible for day-to-day changes in O_3 during winter, whereas variabilities during monsoon arise from multiple competing processes rather than a single dominant factor.
- The O_3 seasonal cycle peaked in June (63.8 ± 5.6 ppbv) unlike the ubiquitous pre-monsoon peak (April-May) observed over the Himalaya and Gangetic regions. The monsoonal dip (July to
- 600 September) is much smaller compared to those observed over the Himalaya region. MDA8 is close to and occasionally crosses the WHO threshold of $100 \mu\text{g m}^{-3}$ during May-June along with higher values of vegetation-related O_3 exposure indices. The photochemistry, fueled by the higher levels of precursors, falling in the NO_x -VOC transition regime leads to higher O_3 values during May-June.
- 605 ● Surface O_3 varied from 39–64 ppbv with seasonal amplitude of 25.5 ppbv, being lower during winter. The CAM-Chem O_3 climatology, after revising stratospheric contribution from CAMS, agrees with the observed seasonal pattern, however, model overestimated wintertime levels by 10–16 ppbv. Nearly half of the O_3 in Trans-Himalaya is contributed by anthropogenic NO_x emissions from South Asia (15–18 %) and outside South Asia (32–37 %) throughout the year.
- 610 From a VOC perspective, nearly half of O_3 is driven by oxidation of CH_4 . Among various sources, the following four major contributors largely shape the observed seasonal pattern over the Trans-Himalaya: CH_4 oxidation, biogenic emissions of NO_x and VOCs, stratospheric O_3 , and anthropogenic NO_x emission from regions outside South Asia. Besides these regional and global photochemical contributions, seasonal peak in O_3 is significantly influenced by stratospheric
- 615 inputs.
- The study can serve as a reference for designing future field experiments and improvement of global and regional models over the Himalayan region. In particular, measurements of NO_x , CH_4 and other VOCs, studying the dynamics enhancing O_3 in the evening hours, and reducing wintertime biases in the model could be crucial. This study also represents the need for
- 620 continuation of O_3 measurements for air quality monitoring as its levels are close to the threshold.

Overall, the study highlights the varying roles of chemistry, dynamics and regional-to-global anthropogenic sources in controlling the O_3 magnitude and variations over the Trans-Himalaya. The rising levels of O_3 and its precursors—with surface O_3 at $1.4 \% \text{ y}^{-1}$, NO_2 at $\sim 7 \% \text{ y}^{-1}$ and HCHO at $\sim 4 \% \text{ y}^{-1}$ —highlight the impact of rapid urbanization and/or tourism, and underscore the need of

625 monitoring of O_3 and its precursors along with high-resolution chemistry-transport modeling over



this climate-sensitive region of Trans-Himalaya. Comprehensive and continuous O₃ monitoring in this data-sparse region can provide crucial insights into unexplored atmospheric chemistry and transport processes, which are hard to obtain through other public health-centric O₃ observations focused only
630 in urban centres across India. Observed higher values of O₃ are sensitive to NO_x as well as VOCs, hence monitoring of various NO_x and VOCs besides other precursors is essential for better quantification of the gradient between local emissions and background levels. With new observation-based insights and evaluation of models, future field studies can be designed more strategically and improve the model simulations to further advance the understanding of
635 atmospheric chemistry and dynamics of the Trans-Himalayan region.

Acknowledgement

We are thankful to India Meteorological Department (IMD) for providing meteorological observations recorded at Leh, Ladakh. We thank Copernicus Atmosphere Monitoring Service (CAMS), ERA-5 reanalysis of the European Center for Medium range Weather Forecasting (ECMWF)
640 for making chemical and meteorological fields from their websites, <https://ads.atmosphere.copernicus.eu/datasets/cams-global-reanalysis-eac4?tab=overview> (last access: 26 May 2026), and <https://cds.climate.copernicus.eu/datasets/reanalysis-era5-pressure-levels?tab=overview> (last access: 26 May 2026), respectively. Cloud cover data of INSAT-3DS was obtained from ISRO's MOSDAC website, <https://www.mosdac.gov.in/catalog/satellite.php?mission=INSAT-3DS> (last access: 26 May 2026). We gratefully acknowledge the Sentinel-5p's TROPOMI observations, which were obtained from <https://developers.google.com/earth-engine/datasets/catalog/sentinel-5p> (last access: 26 May 2026). TA utilized the high-performance computing resources made possible by funding from the Ministry of Science, Research and Culture of the State of Brandenburg (MWFK) and are operated by
650 the IT Services and Operations unit of the Helmholtz Centre Potsdam. TA would like to thank Edward Chan at RIFS for his technical assistance in setting-up the CAM-Chem model on the GFZ GLIC supercluster. We acknowledge use of the WRF-Chem model preprocessor tools (anthro_emis, mozbc, fire_emiss, etc.) provided by the Atmospheric Chemistry Observations and Modeling Lab of NCAR (National Centre for Atmospheric Research), USA. WRF-Chem simulations were performed on
655 the Param Vikram-1000 High Performance Computing Cluster of the Physical Research Laboratory (PRL). This study is supported by Department of Space, Government of India.

Author contributions: IAG and MP conceptualised and designed the study. IAG and SA performed the measurements, with support from AV, LKS, BPS and SS. TA, TB, and NO contributed to the model



660 results and related inputs. IAG led the study and prepared the first draft of the manuscript. All co-
authors contributed to the discussions, reviews, and editing.

Data availability

In situ measured surface O₃ (monthly means) is provided in supplementary (Table S1). Hourly interval O₃ (measured and modelled) will be made available on Zenodo at the acceptance of the paper.

665 Declaration of competing interest

One of the (co-)authors is a member of the editorial board of Atmospheric Chemistry and Physics.

References

Ajayakumar, R. S., Girach, I. A., Soni, M., Ojha, N., and Babu, S. S.: Processes governing the surface ozone over a tropical hill station in the Western Ghats, *Atmos. Environ.*, 319, 120286, 670 <https://doi.org/10.1016/j.atmosenv.2023.120286>, 2024.

Anagha, K. S. and Kuttippurath, J.: Rising ozone pollution as a threat to wheat yield in India: insights from a concentration-based approach, *Environ. Sci. Process. Impacts*, 28, 1047–1063, <https://doi.org/10.1039/D5EM00850F>, 2026.

675 Ansari, T., Nalam, A., Lupaşcu, A., Hinz, C., Grasse, S., and Butler, T.: Explaining trends and changing seasonal cycles of surface ozone in North America and Europe over the 2000–2018 period: a global modelling study with NO_x and VOC tagging, *Atmospheric Chem. Phys.*, 25, 16833–16876, <https://doi.org/10.5194/acp-25-16833-2025>, 2025.

680 Barth, M. C., Lee, J., Hodzic, A., Pfister, G., Skamarock, W. C., Worden, J., Wong, J., and Noone, D.: Thunderstorms and upper troposphere chemistry during the early stages of the 2006 North American Monsoon, *Atmospheric Chem. Phys.*, 12, 11003–11026, <https://doi.org/10.5194/acp-12-11003-2012>, 2012.

Bhan, S. C., Devrani, A. K., and Sinha, V.: An analysis of monthly rainfall and the meteorological conditions associated with cloudburst over the dry region of Leh (Ladakh), India, *MAUSAM*, 66, 107–122, <https://doi.org/10.54302/mausam.v66i1.371>, 2015.

685 Bhattacharjee, D. and Dutta, R. K.: Mountainous Hazards and Sustainable Livelihood in Leh Valley, in: *Indigenous Knowledge and Disaster Risk Reduction*, edited by: Panda, G. K., Chatterjee, U.,



- Bandyopadhyay, N., Setiawati, M. D., and Banerjee, D., Springer International Publishing, Cham, 83–105, https://doi.org/10.1007/978-3-031-26143-5_5, 2023.
- Borsdorff, T., Aan de Brugh, J., Hu, H., Aben, I., Hasekamp, O., and Landgraf, J.: Measuring Carbon Monoxide With TROPOMI: First Results and a Comparison With ECMWF-IFS Analysis Data, *Geophys. Res. Lett.*, 45, 2826–2832, <https://doi.org/10.1002/2018GL077045>, 2018.
- Butler, T., Lupascu, A., and Nalam, A.: Attribution of ground-level ozone to anthropogenic and natural sources of nitrogen oxides and reactive carbon in a global chemical transport model, *Atmospheric Chem. Phys.*, 20, 10707–10731, <https://doi.org/10.5194/acp-20-10707-2020>, 2020.
- 695 Carslaw, K. S., Regayre, L. A., Proske, U., Gettelman, A., Sexton, D. M. H., Qian, Y., Marshall, L., Wild, O., Van Lier-Walqui, M., Oertel, A., Peatier, S., Yang, B., Johnson, J. S., Li, S., McCoy, D. T., Sanderson, B. M., Williamson, C. J., Elsaesser, G. S., Yamazaki, K., and Booth, B. B. B.: Opinion: The importance and future development of perturbed parameter ensembles in climate and atmospheric science, <https://doi.org/10.5194/egusphere-2025-4341>, 17 September 2025.
- 700 Chevalier, A., Gheusi, F., Delmas, R., Ordóñez, C., Sarrat, C., Zbinden, R., Thouret, V., Athier, G., and Cousin, J.-M.: Influence of altitude on ozone levels and variability in the lower troposphere: a ground-based study for western Europe over the period 2001–2004, *Atmospheric Chem. Phys.*, 7, 4311–4326, <https://doi.org/10.5194/acp-7-4311-2007>, 2007.
- Chevuturi, A., Dimri, A. P., and Thayyen, R. J.: Climate change over Leh (Ladakh), India, *Theor. Appl. Climatol.*, 131, 531–545, <https://doi.org/10.1007/s00704-016-1989-1>, 2018.
- 705 Chuwah, C., Van Noije, T., Van Vuuren, D. P., Stehfest, E., and Hazeleger, W.: Global impacts of surface ozone changes on crop yields and land use, *Atmos. Environ.*, 106, 11–23, <https://doi.org/10.1016/j.atmosenv.2015.01.062>, 2015.
- Crippa, M., Guizzardi, D., Oreggioni, G., Muntean, M., and Schaaf, E.: EDGARv5.0 Air Pollutant Emissions, <https://doi.org/10.1594/PANGAEA.921922>, 2020.
- 710 Crippa, M., Guizzardi, D., Butler, T., Keating, T., Wu, R., Kaminski, J., Kuenen, J., Kurokawa, J., Chatani, S., Morikawa, T., Pouliot, G., Racine, J., Moran, M. D., Klimont, Z., Manseau, P. M., Mashayekhi, R., Henderson, B. H., Smith, S. J., Suchyta, H., Muntean, M., Solazzo, E., Banja, M., Schaaf, E., Pagani, F., Woo, J.-H., Kim, J., Monforti-Ferrario, F., Pisoni, E., Zhang, J., Niemi, D., Sassi, M., Ansari, T., and Foley, K.: The HTAP_v3 emission mosaic: merging regional and global monthly



- emissions (2000–2018) to support air quality modelling and policies, *Earth Syst. Sci. Data*, **15**, 2667–2694, <https://doi.org/10.5194/essd-15-2667-2023>, 2023.
- Cristofanelli, P., Bracci, A., Sprenger, M., Marinoni, A., Bonafè, U., Calzolari, F., Duchi, R., Laj, P., Pichon, J. M., Roccatò, F., Venzac, H., Vuilleumoz, E., and Bonasoni, P.: Tropospheric ozone variations
720 at the Nepal Climate Observatory-Pyramid (Himalayas, 5079 m a.s.l.) and influence of deep stratospheric intrusion events, *Atmospheric Chem. Phys.*, **10**, 6537–6549, <https://doi.org/10.5194/acp-10-6537-2010>, 2010.
- Das, S., Giorgi, F., Coppola, E., Panicker, A. S., Gautam, A. S., Nair, V. S., and Giuliani, G.: Linkage
725 between the absorbing aerosol-induced snow darkening effects over the Himalayas-Tibetan Plateau and the pre-monsoon climate over northern India, *Theor. Appl. Climatol.*, **147**, 1033–1048, <https://doi.org/10.1007/s00704-021-03871-y>, 2022.
- De Smedt, I., Theys, N., Yu, H., Danckaert, T., Lerot, C., Compernelle, S., Van Roozendaal, M., Richter, A., Hilboll, A., Peters, E., Pedergnana, M., Loyola, D., Beirle, S., Wagner, T., Eskes, H., Van Geffen, J., Boersma, K. F., and Veefkind, P.: Algorithm theoretical baseline for formaldehyde retrievals from S5P
730 TROPOMI and from the QA4ECV project, *Atmospheric Meas. Tech.*, **11**, 2395–2426, <https://doi.org/10.5194/amt-11-2395-2018>, 2018.
- Dolma, Y.: Tourism in Ladakh: Trends and composition, *International Journal of Research in Social Sciences*, **10** (12), https://www.ijmra.us/project%20doc/2020/IJRSS_DECEMBER2020/IJRSS12Dec20-21086.pdf, 2020.
- 735 Dubey, J., Singh, D. S., and Sati, S. P.: Cryosphere Response to Climate Change and Disaster Risk Reduction in the Arid Northwestern Ladakh Himalaya, in: *Ecosystem-based Approaches for Resilience Building in Himalayan Landscapes*, edited by: Khan, Y. D. I., Goswami, M., and Nautiyal, S., Springer Nature Singapore, Singapore, 3–27, https://doi.org/10.1007/978-981-95-2007-7_1, 2025.
- Emmerichs, T., Kerkweg, A., Ouwersloot, H., Fares, S., Mammarella, I., and Taraborrelli, D.: A revised
740 dry deposition scheme for land–atmosphere exchange of trace gases in ECHAM/MESy v2.54, *Geosci. Model Dev.*, **14**, 495–519, <https://doi.org/10.5194/gmd-14-495-2021>, 2021.
- Emmons, L. K., Walters, S., Hess, P. G., Lamarque, J.-F., Pfister, G. G., Fillmore, D., Granier, C., Guenther, A., Kinnison, D., Laepple, T., Orlando, J., Tie, X., Tyndall, G., Wiedinmyer, C., Baughcum, S. L., and Kloster, S.: Description and evaluation of the Model for Ozone and Related chemical Tracers, version 4 (MOZART-4), *Geosci. Model Dev.*, **3**, 43–67, <https://doi.org/10.5194/gmd-3-43-2010>, 2010.
- 745



- Fuhrer, J., Skärby, L., and Ashmore, M. R.: Critical levels for ozone effects on vegetation in Europe, *Environ. Pollut.*, 97, 91–106, [https://doi.org/10.1016/S0269-7491\(97\)00067-5](https://doi.org/10.1016/S0269-7491(97)00067-5), 1997.
- Gao, Y., Kou, W., Cheng, W., Guo, X., Qu, B., Wu, Y., Zhang, S., Liao, H., Chen, D., Leung, L. R., Wild, O., Zhang, J., Lin, G., Su, H., Cheng, Y., Pöschl, U., Pozzer, A., Zhang, L., Lamarque, J., Guenther, A. B.,
750 Brasseur, G., Liu, Z., Lu, H., Li, C., Zhao, B., Wang, S., Huang, X., Pan, J., Liu, G., Liu, X., Lin, H., Zhao, Y.,
Zhao, C., Meng, J., Yao, X., Gao, H., and Wu, L.: Reducing Long-Standing Surface Ozone
Overestimation in Earth System Modeling by High-Resolution Simulation and Dry Deposition
Improvement, *J. Adv. Model. Earth Syst.*, 17, e2023MS004192,
<https://doi.org/10.1029/2023MS004192>, 2025.
- 755 Gaudel, A., Bourgeois, I., Li, M., Chang, K.-L., Ziemke, J., Sauvage, B., Stauffer, R. M., Thompson, A.
M., Kollonige, D. E., Smith, N., Hubert, D., Keppens, A., Cuesta, J., Heue, K.-P., Veeffkind, P., Aikin, K.,
Peischl, J., Thompson, C. R., Ryerson, T. B., Frost, G. J., McDonald, B. C., and Cooper, O. R.: Tropical
tropospheric ozone distribution and trends from in situ and satellite data, *Atmospheric Chem. Phys.*,
24, 9975–10000, <https://doi.org/10.5194/acp-24-9975-2024>, 2024.
- 760 Gettelman, A., Mills, M. J., Kinnison, D. E., Garcia, R. R., Smith, A. K., Marsh, D. R., Tilmes, S., Vitt, F.,
Bardeen, C. G., McInerney, J., Liu, H. -L., Solomon, S. C., Polvani, L. M., Emmons, L. K., Lamarque, J. -F.,
Richter, J. H., Glanville, A. S., Bacmeister, J. T., Phillips, A. S., Neale, R. B., Simpson, I. R., DuVivier, A.
K., Hodzic, A., and Randel, W. J.: The Whole Atmosphere Community Climate Model Version 6
(WACCM6), *J. Geophys. Res. Atmospheres*, 124, 12380–12403,
765 <https://doi.org/10.1029/2019JD030943>, 2019.
- Ghude, S. D., Kalita, G., Jat, R., Govardhan, G., Debnath, S., Yadav, P. P., Ambulkar, R., Kumar, R., and
Attri, S. D.: The role of atmospheric feedback and groundwater conservation policies in degrading air
quality in Delhi, *Npj Clean Air*, 1, 12, <https://doi.org/10.1038/s44407-025-00012-x>, 2025.
- Girach, I. A., Ojha, N., Nair, P. R., Pozzer, A., Tiwari, Y. K., Kumar, K. R., and Lelieveld, J.: Variations in
770 O₃, CO, and CH₄ over the Bay of Bengal during the summer monsoon season: shipborne
measurements and model simulations, *Atmospheric Chem. Phys.*, 17, 257–275,
<https://doi.org/10.5194/acp-17-257-2017>, 2017.
- Goodrich, C. G., Udas, P. B., and Larrington-Spencer, H.: Conceptualizing gendered vulnerability to
climate change in the Hindu Kush Himalaya: Contextual conditions and drivers of change, *Environ.*
775 *Dev.*, 31, 9–18, <https://doi.org/10.1016/j.envdev.2018.11.003>, 2019.



- Grell, G. A. and Dévényi, D.: A generalized approach to parameterizing convection combining ensemble and data assimilation techniques, *Geophys. Res. Lett.*, 29, <https://doi.org/10.1029/2002GL015311>, 2002.
- 780 Grell, G. A., Peckham, S. E., Schmitz, R., McKeen, S. A., Frost, G., Skamarock, W. C., and Eder, B.: Fully coupled “online” chemistry within the WRF model, *Atmos. Environ.*, 39, 6957–6975, <https://doi.org/10.1016/j.atmosenv.2005.04.027>, 2005.
- Guenther, A., Karl, T., Harley, P., Wiedinmyer, C., Palmer, P. I., and Geron, C.: Estimates of global terrestrial isoprene emissions using MEGAN (Model of Emissions of Gases and Aerosols from Nature), *Atmospheric Chem. Phys.*, 6, 3181–3210, <https://doi.org/10.5194/acp-6-3181-2006>, 2006.
- 785 Harithasree, S., Sharma, K., Girach, I. A., Sahu, L. K., Nair, P. R., Singh, N., Flemming, J., Babu, S. S., and Ojha, N.: Surface ozone over Doon valley of the Indian Himalaya: Characteristics, impact assessment, and model results, *Atmospheric Environ. X*, 21, 100247, <https://doi.org/10.1016/j.aeaoa.2024.100247>, 2024.
- 790 Hassan, M. A., Mehmood, T., Liu, J., Luo, X., Li, X., Tanveer, M., Faheem, M., Shakoore, A., Dar, A. A., and Abid, M.: A review of particulate pollution over Himalaya region: Characteristics and salient factors contributing ambient PM pollution, *Atmos. Environ.*, 294, 119472, <https://doi.org/10.1016/j.atmosenv.2022.119472>, 2023.
- 795 Hersbach, H., Bell, B., Berrisford, P., Hirahara, S., Horányi, A., Muñoz-Sabater, J., Nicolas, J., Peubey, C., Radu, R., Schepers, D., Simmons, A., Soci, C., Abdalla, S., Abellan, X., Balsamo, G., Bechtold, P., Biavati, G., Bidlot, J., Bonavita, M., De Chiara, G., Dahlgren, P., Dee, D., Diamantakis, M., Dragani, R., Flemming, J., Forbes, R., Fuentes, M., Geer, A., Haimberger, L., Healy, S., Hogan, R. J., Hólm, E., Janisková, M., Keeley, S., Laloyaux, P., Lopez, P., Lupu, C., Radnoti, G., De Rosnay, P., Rozum, I., Vamborg, F., Villaume, S., and Thépaut, J.: The ERA5 global reanalysis, *Q. J. R. Meteorol. Soc.*, 146, 1999–2049, <https://doi.org/10.1002/qj.3803>, 2020.
- 800 Hogsett, W. E., Tingey, D. T., and Lee, E. H.: Ozone Exposure Indices: Concepts for Development and Evaluation of their Use, in: *Assessment of Crop Loss From Air Pollutants*, edited by: Heck, W. W., Taylor, O. C., and Tingey, D. T., Springer Netherlands, Dordrecht, 107–138, https://doi.org/10.1007/978-94-009-1367-7_7, 1988.



Hong, S.-Y., Noh, Y., and Dudhia, J.: A New Vertical Diffusion Package with an Explicit Treatment of
805 Entrainment Processes, *Mon. Weather Rev.*, 134, 2318–2341, <https://doi.org/10.1175/MWR3199.1>,
2006.

Huijnen, V., Williams, J., Van Weele, M., Van Noije, T., Krol, M., Dentener, F., Segers, A., Houweling,
S., Peters, W., De Laat, J., Boersma, F., Bergamaschi, P., Van Velthoven, P., Le Sager, P., Eskes, H.,
Alkemade, F., Scheele, R., Nédélec, P., and Pätz, H.-W.: The global chemistry transport model TM5:
810 description and evaluation of the tropospheric chemistry version 3.0, *Geosci. Model Dev.*, 3, 445–
473, <https://doi.org/10.5194/gmd-3-445-2010>, 2010.

Inness, A., Ades, M., Agustí-Panareda, A., Barré, J., Benedictow, A., Blechschmidt, A.-M., Dominguez,
J. J., Engelen, R., Eskes, H., Flemming, J., Huijnen, V., Jones, L., Kipling, Z., Massart, S., Parrington, M.,
Peuch, V.-H., Razinger, M., Remy, S., Schulz, M., and Suttie, M.: The CAMS reanalysis of atmospheric
815 composition, *Atmospheric Chem. Phys.*, 19, 3515–3556, <https://doi.org/10.5194/acp-19-3515-2019>,
2019.

Jiao, G., Chen, L., Li, K., Zhu, J., Dong, X., Zhu, X., Yang, Y., Yue, X., and Liao, H.: Worsened Ozone
Pollution Exacerbates the Loss of Agricultural Production in China, *J. Geophys. Res. Atmospheres*,
130, e2024JD042781, <https://doi.org/10.1029/2024JD042781>, 2025.

820 Jin, X., Fiore, A. M., Murray, L. T., Valin, L. C., Lamsal, L. N., Duncan, B., Folkert Boersma, K., De
Smedt, I., Abad, G. G., Chance, K., and Tonnesen, G. S.: Evaluating a Space-Based Indicator of Surface
Ozone-NO_x-VOC Sensitivity Over Midlatitude Source Regions and Application to Decadal Trends, *J.*
Geophys. Res. Atmospheres, 122, <https://doi.org/10.1002/2017JD026720>, 2017.

Kaylor, S. D., Snell Taylor, S. J., and Herrick, J. D.: Estimates of biomass reductions of ozone sensitive
825 herbaceous plants in California, *Sci. Total Environ.*, 878, 163134,
<https://doi.org/10.1016/j.scitotenv.2023.163134>, 2023.

Khanday, A. A., Rather, G. M., Kumar, M. A., and Lone, A. H.: Environmental Sustainability and Its
Impact on Public Health in Ladakh-India, in: *Sustainability and Health Informatics*, edited by: Tripathi,
G., Shakya, A., Kanga, S., Guite, L. T. S., and Singh, S. K., Springer Nature Singapore, Singapore, 183–
830 198, https://doi.org/10.1007/978-981-97-6706-9_9, 2024.

Kumar, R., Naja, M., Venkataramani, S., and Wild, O.: Variations in surface ozone at Nainital: A high-
altitude site in the central Himalayas, *J. Geophys. Res. Atmospheres*, 115, 2009JD013715,
<https://doi.org/10.1029/2009JD013715>, 2010.



835 Kumar, R., Naja, M., Pfister, G. G., Barth, M. C., and Brasseur, G. P.: Simulations over South Asia using
the Weather Research and Forecasting model with Chemistry (WRF-Chem): set-up and
meteorological evaluation, *Geosci. Model Dev.*, 5, 321–343, <https://doi.org/10.5194/gmd-5-321-2012>, 2012.

Lal, S., Peshin, S. K., Naja, M., and Venkataramani, S.: Variability of Ozone and Related Trace Gases
Over India, in: *Observed Climate Variability and Change over the Indian Region*, edited by: Rajeevan,
840 M. N. and Nayak, S., Springer Singapore, Singapore, 249–269, https://doi.org/10.1007/978-981-10-2531-0_14, 2017.

Landgraf, J., Aan De Brugh, J., Scheepmaker, R., Borsdorff, T., Hu, H., Houweling, S., Butz, A., Aben, I.,
and Hasekamp, O.: Carbon monoxide total column retrievals from TROPOMI shortwaveinfrared
measurements, *Atmospheric Meas. Tech.*, 9, 4955–4975, <https://doi.org/10.5194/amt-9-4955-2016>,
845 2016.

Lee, E. H., Tingey, D. T., and Hogsett, W. E.: Evaluation of ozone exposure indices in exposure-
response modeling, *Environ. Pollut.*, 53, 43–62, [https://doi.org/10.1016/0269-7491\(88\)90024-3](https://doi.org/10.1016/0269-7491(88)90024-3),
1988.

Lee, J., Han, J., Park, J., Ahn, J.-Y., and Lee, G.: Long-term changes of rice yield loss estimated with
850 AOT40 and M7 metrics using comprehensive ozone and rice cultivation data over South Korea, *Asian
J. Atmospheric Environ.*, 17, 21, <https://doi.org/10.1007/s44273-023-00021-w>, 2023.

Lefohn, A. S. and Runeckles, V. C.: Establishing standards to protect vegetation—ozone
exposure/dose considerations, *Atmospheric Environ.* 1967, 21, 561–568,
[https://doi.org/10.1016/0004-6981\(87\)90038-2](https://doi.org/10.1016/0004-6981(87)90038-2), 1987.

855 Liao, Z., Zhang, J., Gao, M., and Ma, Z.: Widespread stratospheric intrusion influence on summer
ozone pollution over China revealed by multi-site ozonesonde and validated EAC4 reanalysis,
Atmospheric Chem. Phys., 25, 14865–14877, <https://doi.org/10.5194/acp-25-14865-2025>, 2025.

Liu, Z., Doherty, R. M., Wild, O., O'Connor, F. M., and Turnock, S. T.: Correcting ozone biases in a
global chemistry–climate model: implications for future ozone, *Atmospheric Chem. Phys.*, 22,
860 12543–12557, <https://doi.org/10.5194/acp-22-12543-2022>, 2022.

Lu, X., Liu, Y., Su, J., Weng, X., Ansari, T., Zhang, Y., He, G., Zhu, Y., Wang, H., Zeng, G., Li, J., He, C., Li,
S., Amnuaylojaroen, T., Butler, T., Fan, Q., Fan, S., Forster, G. L., Gao, M., Hu, J., Kanaya, Y., Latif, M.
T., Lu, K., Nédélec, P., Nowack, P., Sauvage, B., Xu, X., Zhang, L., Li, K., Koo, J.-H., and Nagashima, T.:



865 Tropospheric ozone trends and attributions over East and Southeast Asia in 1995–2019: an
integrated assessment using statistical methods, machine learning models, and multiple chemical
transport models, *Atmospheric Chem. Phys.*, 25, 7991–8028, <https://doi.org/10.5194/acp-25-7991-2025>, 2025.

Mahata, K. S., Rupakheti, M., Panday, A. K., Bhardwaj, P., Naja, M., Singh, A., Mues, A., Cristofanelli,
P., Pudasainee, D., Bonasoni, P., and Lawrence, M. G.: Observation and analysis of spatiotemporal
870 characteristics of surface ozone and carbon monoxide at multiple sites in the Kathmandu Valley,
Nepal, *Atmospheric Chem. Phys.*, 18, 14113–14132, <https://doi.org/10.5194/acp-18-14113-2018>,
2018.

Martin, R. V., Fiore, A. M., and Van Donkelaar, A.: Space-based diagnosis of surface ozone sensitivity
to anthropogenic emissions, *Geophys. Res. Lett.*, 31, 2004GL019416,
875 <https://doi.org/10.1029/2004GL019416>, 2004.

Mills, G., Buse, A., Gimeno, B., Bermejo, V., Holland, M., Emberson, L., and Pleijel, H.: A synthesis of
AOT40-based response functions and critical levels of ozone for agricultural and horticultural crops,
Atmos. Environ., 41, 2630–2643, <https://doi.org/10.1016/j.atmosenv.2006.11.016>, 2007.

Miyazaki, K., Marchetti, Y., Montgomery, J., Lu, S., and Bowman, K.: Identifying drivers of surface
880 ozone bias in global chemical reanalysis with explainable machine learning, *Atmospheric Chem.
Phys.*, 25, 8507–8532, <https://doi.org/10.5194/acp-25-8507-2025>, 2025.

Mogno, C. and Marvin, M. R.: EDGAR v5.0 emissions inventory speciated for the MOZART chemical
mechanism (v1.0.0), <https://doi.org/10.5281/ZENODO.6130621>, 2022.

Nair, P. R., Ajayakumar, R. S., David, L. M., Girach, I. A., and Mottungan, K.: Decadal changes in
885 surface ozone at the tropical station Thiruvananthapuram (8.542° N, 76.858° E), India: effects of
anthropogenic activities and meteorological variability, *Environ. Sci. Pollut. Res.*, 25, 14827–14843,
<https://doi.org/10.1007/s11356-018-1695-x>, 2018.

Nair, V. S., Usha, K. H., and Babu, S. S.: Elevation-dependence of warming due to aerosol-induced
snow darkening over the Himalayan-Tibetan region, *Environ. Res. Lett.*, 19, 014049,
890 <https://doi.org/10.1088/1748-9326/ad1346>, 2024.

Naja, M.: Diurnal and seasonal variabilities in surface ozone at a high altitude site Mt Abu (24.6°N,
72.7°E, 1680m asl) in India, *Atmos. Environ.*, 37, 4205–4215, [https://doi.org/10.1016/S1352-2310\(03\)00565-X](https://doi.org/10.1016/S1352-2310(03)00565-X), 2003.



895 Nalam, A., Lupaşcu, A., Ansari, T., and Butler, T.: Regional and sectoral contributions of NO_x and reactive carbon emission sources to global trends in tropospheric ozone during the 2000–2018 period, *Atmospheric Chem. Phys.*, 25, 5287–5311, <https://doi.org/10.5194/acp-25-5287-2025>, 2025.

900 Ningombam, S. S., Bagare, S. P., Srivastava, A. K., Kanawade, V. P., Singh, R. B., and Padhy, S. K.: Temporal asymmetry in aerosol optical characteristics: A case study at a high-altitude station, Hanle, in Ladakh region, *J. Atmospheric Sol.-Terr. Phys.*, 121, 123–131, <https://doi.org/10.1016/j.jastp.2014.10.012>, 2014.

Ojha, N., Naja, M., Singh, K. P., Sarangi, T., Kumar, R., Lal, S., Lawrence, M. G., Butler, T. M., and Chandola, H. C.: Variabilities in ozone at a semi-urban site in the Indo-Gangetic Plain region: Association with the meteorology and regional processes, *J. Geophys. Res. Atmospheres*, 117, 2012JD017716, <https://doi.org/10.1029/2012JD017716>, 2012.

905 Ojha, N., Girach, I., Sharma, K., Nair, P., Singh, J., Sharma, N., Singh, N., Flemming, J., Inness, A., and Subrahmanyam, K. V.: Surface ozone in the Doon Valley of the Himalayan foothills during spring, *Environ. Sci. Pollut. Res.*, 26, 19155–19170, <https://doi.org/10.1007/s11356-019-05085-2>, 2019.

910 Ojha, N., Girach, I., Soni, M., and Singh, N.: Distribution of reactive trace gases over South Asia: Observations and modeling, in: *Asian Atmospheric Pollution*, Elsevier, 147–169, <https://doi.org/10.1016/B978-0-12-816693-2.00022-6>, 2022.

Okamoto, S. and Tanimoto, H.: A review of atmospheric chemistry observations at mountain sites, *Prog. Earth Planet. Sci.*, 3, 34, <https://doi.org/10.1186/s40645-016-0109-2>, 2016.

915 Otte, T. L.: The Impact of Nudging in the Meteorological Model for Retrospective Air Quality Simulations. Part I: Evaluation against National Observation Networks, *J. Appl. Meteorol. Climatol.*, 47, 1853–1867, <https://doi.org/10.1175/2007JAMC1790.1>, 2008.

Pandit, M. K.: The Himalayas must be protected, *Nature*, 501, 283–283, <https://doi.org/10.1038/501283a>, 2013.

920 Park, S., Son, S.-W., Jung, M.-I., Park, J., and Park, S. S.: Evaluation of tropospheric ozone reanalyses with independent ozonesonde observations in East Asia, *Geosci. Lett.*, 7, 12, <https://doi.org/10.1186/s40562-020-00161-9>, 2020.

Prather, M. J. and Zhu, X.: Lifetimes and timescales of tropospheric ozone, *Elem Sci Anth*, 12, 00112, <https://doi.org/10.1525/elementa.2023.00112>, 2024.



- Putero, D., Cristofanelli, P., Marinoni, A., Adhikary, B., Duchi, R., Shrestha, S. D., Verza, G. P., Landi, T. C., Calzolari, F., Busetto, M., Agrillo, G., Biancofiore, F., Di Carlo, P., Panday, A. K., Rupakheti, M., and Bonasoni, P.: Seasonal variation of ozone and black carbon observed at Paknajol, an urban site in the Kathmandu Valley, Nepal, *Atmospheric Chem. Phys.*, 15, 13957–13971, <https://doi.org/10.5194/acp-15-13957-2015>, 2015.
- Ren, J., Guo, F., and Xie, S.: Diagnosing ozone–NO_x–VOC sensitivity and revealing causes of ozone increases in China based on 2013–2021 satellite retrievals, *Atmospheric Chem. Phys.*, 22, 15035–15047, <https://doi.org/10.5194/acp-22-15035-2022>, 2022.
- Romatschke, U. and Houze, R. A.: Characteristics of Precipitating Convective Systems in the South Asian Monsoon, *J. Hydrometeorol.*, 12, 3–26, <https://doi.org/10.1175/2010JHM1289.1>, 2011.
- Sahu, L. K., Lal, S., Thouret, V., and Smit, H. G.: Seasonality of tropospheric ozone and water vapor over Delhi, India: a study based on MOZAIC measurement data, *J. Atmospheric Chem.*, 62, 151–174, <https://doi.org/10.1007/s10874-010-9146-1>, 2009.
- Santra, P.: Scope of Solar Energy in Cold Arid Region of India at Leh Ladakh, *Ann. Arid Zone*, 54, <https://doi.org/10.56093/aaz.v54i3-4.63046>, 2016.
- Saraf, N. and Beig, G.: Long-term trends in tropospheric ozone over the Indian tropical region, *Geophys. Res. Lett.*, 31, 2003GL018516, <https://doi.org/10.1029/2003GL018516>, 2004.
- Sarang, T., Naja, M., Ojha, N., Kumar, R., Lal, S., Venkataramani, S., Kumar, A., Sagar, R., and Chandola, H. C.: First simultaneous measurements of ozone, CO, and NO_y at a high-altitude regional representative site in the central Himalayas, *J. Geophys. Res. Atmospheres*, 119, 1592–1611, <https://doi.org/10.1002/2013JD020631>, 2014.
- Seinfeld, J. H. and Pandis, S. N.: *Atmospheric Chemistry and Physics: From Air Pollution to Climate Change*, 1st ed., John Wiley & Sons, Incorporated, Newark, 1 pp., 2016.
- Sharma, A., Ojha, N., Pozzer, A., Mar, K. A., Beig, G., Lelieveld, J., and Gunthe, S. S.: WRF-Chem simulated surface ozone over south Asia during the pre-monsoon: effects of emission inventories and chemical mechanisms, *Atmospheric Chem. Phys.*, 17, 14393–14413, <https://doi.org/10.5194/acp-17-14393-2017>, 2017.



950 Sharma, P., Kuniyal, J. C., Chand, K., Guleria, R. P., Dhyani, P. P., and Chauhan, C.: Surface ozone concentration and its behaviour with aerosols in the northwestern Himalaya, India, *Atmos. Environ.*, 71, 44–53, <https://doi.org/10.1016/j.atmosenv.2012.12.042>, 2013.

Sindelarova, K., Markova, J., Simpson, D., Huszar, P., Karlicky, J., Darras, S., and Granier, C.: High-resolution biogenic global emission inventory for the time period 2000–2019 for air quality
955 modelling, *Earth Syst. Sci. Data*, 14, 251–270, <https://doi.org/10.5194/essd-14-251-2022>, 2022.

Singh, J., Singh, N., Ojha, N., Sharma, A., Pozzer, A., Kiran Kumar, N., Rajeev, K., Gunthe, S. S., and Kotamarthi, V. R.: Effects of spatial resolution on WRF v3.8.1 simulated meteorology over the central Himalaya, *Geosci. Model Dev.*, 14, 1427–1443, <https://doi.org/10.5194/gmd-14-1427-2021>, 2021.

Sinha, P. R., Sahu, L. K., Manchanda, R. K., Sheel, V., Deushi, M., Kajino, M., Schultz, M. G., Nagendra,
960 N., Kumar, P., Trivedi, D. B., Koli, S. K., Peshin, S. K., Swamy, Y. V., Tzanis, C. G., and Sreenivasan, S.: Transport of tropospheric and stratospheric ozone over India: Balloon-borne observations and modeling analysis, *Atmos. Environ.*, 131, 228–242, <https://doi.org/10.1016/j.atmosenv.2016.02.001>, 2016.

Škerlak, B., Sprenger, M., and Wernli, H.: A global climatology of stratosphere–troposphere
965 exchange using the ERA-Interim data set from 1979 to 2011, *Atmospheric Chem. Phys.*, 14, 913–937, <https://doi.org/10.5194/acp-14-913-2014>, 2014.

Tanimoto, H., Mukai, H., Sawa, Y., Matsueda, H., Yonemura, S., Wang, T., Poon, S., Wong, A., Lee, G.,
Jung, J. Y., Kim, K. R., Lee, M. H., Lin, N. H., Wang, J. L., Ou-Yang, C. F., Wu, C. F., Akimoto, H.,
Pochanart, P., Tsuboi, K., Doi, H., Zellweger, C., and Klausen, J.: Direct assessment of international
970 consistency of standards for ground-level ozone: strategy and implementation toward metrological traceability network in Asia, *J. Environ. Monit.*, 9, 1183, <https://doi.org/10.1039/b701230f>, 2007.

Tilmes, S., Lamarque, J.-F., Emmons, L. K., Kinnison, D. E., Ma, P.-L., Liu, X., Ghan, S., Bardeen, C.,
Arnold, S., Deeter, M., Vitt, F., Ryerson, T., Elkins, J. W., Moore, F., Spackman, J. R., and Val Martin,
M.: Description and evaluation of tropospheric chemistry and aerosols in the Community Earth
975 System Model (CESM1.2), *Geosci. Model Dev.*, 8, 1395–1426, <https://doi.org/10.5194/gmd-8-1395-2015>, 2015.

Tsutsumi, Y., Zaizen, Y., and Makino, Y.: Tropospheric ozone measurement at the top of Mt. Fuji, *Geophys. Res. Lett.*, 21, 1727–1730, <https://doi.org/10.1029/94GL01107>, 1994.



Turnock, S. T., Akritidis, D., Horowitz, L., Mertens, M., Pozzer, A., Reddington, C. L., Wang, H., Zhou,
980 P., and O'Connor, F.: Drivers of change in peak-season surface ozone concentrations and impacts on
human health over the historical period (1850–2014), *Atmospheric Chem. Phys.*, 25, 7111–7136,
<https://doi.org/10.5194/acp-25-7111-2025>, 2025.

Udayasoorian, C., Jayabalakrishnan, R. M., Suguna, A. R., Venkataramani, S., and Lal, S.: Diurnal and
seasonal characteristics of ozone and NO_x over a high-altitude western Ghats location in southern
985 India, *Advances in Applied Science Research*, 4(5):309-320, 2013.

US EPA: Integrated Science Assessment (ISA) for Ozone and Related Photochemical Oxidants
(<https://assessments.epa.gov/isa/document/&deid%3D247492>), 2013.

Van Der Werf, G. R., Randerson, J. T., Giglio, L., Collatz, G. J., Mu, M., Kasibhatla, P. S., Morton, D. C.,
DeFries, R. S., Jin, Y., and Van Leeuwen, T. T.: Global fire emissions and the contribution of
990 deforestation, savanna, forest, agricultural, and peat fires (1997–2009), *Atmospheric Chem. Phys.*,
10, 11707–11735, <https://doi.org/10.5194/acp-10-11707-2010>, 2010.

Van Geffen, J., Eskes, H., Compernelle, S., Pinardi, G., Verhoelst, T., Lambert, J.-C., Sneep, M., Ter
Linden, M., Ludewig, A., Boersma, K. F., and Veeffkind, J. P.: Sentinel-5P TROPOMI NO₂ retrieval:
impact of version v2.2 improvements and comparisons with OMI and ground-based data,
995 *Atmospheric Meas. Tech.*, 15, 2037–2060, <https://doi.org/10.5194/amt-15-2037-2022>, 2022.

Wester, P., Mishra, A., Mukherji, A., and Shrestha, A. B. (Eds.): *The Hindu Kush Himalaya Assessment: Mountains, Climate Change, Sustainability and People*, Springer International Publishing, Cham,
<https://doi.org/10.1007/978-3-319-92288-1>, 2019.

WHO: WHO global air quality guidelines: particulate matter (PM_{2.5} and PM₁₀), ozone, nitrogen
1000 dioxide, sulfur dioxide and carbon monoxide
(<https://www.who.int/publications/i/item/9789240034228>), 2021.

Wiedinmyer, C., Kimura, Y., McDonald-Buller, E. C., Emmons, L. K., Buchholz, R. R., Tang, W., Seto, K.,
Joseph, M. B., Barsanti, K. C., Carlton, A. G., and Yokelson, R.: The Fire Inventory from NCAR version
2.5: an updated global fire emissions model for climate and chemistry applications, *Geosci. Model*
1005 *Dev.*, 16, 3873–3891, <https://doi.org/10.5194/gmd-16-3873-2023>, 2023.

Wild, O. and Ryan, E. M.: Quantifying and addressing the uncertainties in tropospheric ozone and OH
in a global chemistry transport model, *Atmospheric Chem. Phys.*, 26, 2255–2273,
<https://doi.org/10.5194/acp-26-2255-2026>, 2026.



1010 Yongde, K. and Xinchun, L.: Characteristics and potential source areas of ozone pollution in Pamir Plateau, *Sci. Total Environ.*, 967, 178783, <https://doi.org/10.1016/j.scitotenv.2025.178783>, 2025.

Zaveri, R. A., Easter, R. C., Fast, J. D., and Peters, L. K.: Model for Simulating Aerosol Interactions and Chemistry (MOSAIC), *J. Geophys. Res. Atmospheres*, 113, 2007JD008782, <https://doi.org/10.1029/2007JD008782>, 2008.

1015 Ziegler, A. D., Cantarero, S. I., Wasson, R. J., Srivastava, P., Spalzin, S., Chow, W. T. L., and Gillen, J.: A clear and present danger: Ladakh's increasing vulnerability to flash floods and debris flows, *Hydrol. Process.*, 30, 4214–4223, <https://doi.org/10.1002/hyp.10919>, 2016.